Journal of Molecular Liquids 391 (2023) 123242

Contents lists available at ScienceDirect

Journal of Molecular Liquids

journal homepage: www.elsevier.com/locate/molliq

# Molecular hybrids integrated with imidazole and hydrazone structural motifs: Design, synthesis, biological evaluation, and molecular docking studies

Michael Tapera [a,*], Hüseyin Kekeçmuhammed [a], Emin Sarıpınar [a,*], Murat Doğan [b], Burak Tüzün [c], Ümit M. Koçyiğit [d], Feyza Nur Çetin [d]

[a] Department of Chemistry, Erciyes University, Kayseri, Turkey
[b] Department of Pharmaceutical Biotechnology, Sivas Cumhuriyet University, Sivas, Turkey
[c] Department of Plant and Animal Production, Sivas Cumhuriyet University, Sivas, Turkey
[d] Department of Basic Pharmaceutical Sciences, Sivas Cumhuriyet University, Sivas, Turkey

ARTICLE INFO

*Keywords:*
Imidazole
Synthesis
Enzyme inhibition
Cytotoxic activity
Molecular docking
ADME/T

ABSTRACT

In the present work, a series of compounds containing imidazole and hydrazone structural frameworks were synthesized and characterized using various spectral techniques, including $^{1}H$ NMR, $^{13}C$ NMR, FTIR, and HRMS. Synthesized compounds were subjected to screening as antiproliferative agents as well as against two physiologically and pharmacologically relevant human carbonic anhydrase (hCA) isoforms: hCA I and hCA II. Among them, some compounds exhibited remarkable antiproliferative activity with less cytotoxicity activity to healthy cells and significant CA inhibitory activities in contrast to a standard inhibitor with Ki values in the range of 0.49 ± 1.010–739.12 ± 111.35 nM for hCA I (Ki value for standard inhibitor = 271.15 ± 74.620 nM), 64.53 ± 19.44–314.37 ± 54.78 nM for hCA II (Ki value for standard inhibitor = 113.07 ± 20.980 nM). In addition, DFT calculations were performed to get insight into the distinctive reactive sites of all compounds, and subsequently, the reactive centers of the compounds were determined. Moreover, molecular docking studies of the most potent compounds were conducted, and results showed reasonable binding modes in the active sites of hCA I protein (PDB ID: 2CAB), hCA II protein (PDB ID: 3DC3), as well as colon cancer protein (PDB ID: 4UYA and 3DTC). Finally, in silico predictions of ADME and pharmacokinetic parameters indicated that these compounds should have good oral bioavailability.

## 1. Introduction

Cancer is the second-leading cause of mortality worldwide, after cardiovascular diseases. According to the World Health Organization (WHO), cancer is expected to kill 12 million people worldwide by 2030 [1]. Therefore, researchers and pharmaceutical companies have made finding and developing new, effective cancer treatments a top priority. Existing chemotherapeutic drugs can kill cancerous cells, but they are not 100% successful. They are becoming less effective due to the development of drug resistance by cancer cells. In addition, long-term use of these previously reported chemotherapeutic drugs can cause hepatotoxicity, myelotoxicity, neurotoxicity, urinary toxicity, and cardiac toxicity [2,3]. As a result, several research organizations throughout the world are attempting to produce effective anticancer drugs with minimal side effects and high efficacy [4].

The enzyme carbonic anhydrase (CA) is a zinc-containing enzyme that is ubiquitous in nature. This enzyme catalyzes an important biological reaction: the reversible hydration of carbon dioxide (CO2) to a bicarbonate ion (HCO3–) and a proton (H+) [5]. CA inhibitors, including acetazolamide, brinzolamide, brimonidine, diclofenamide, etc., suppress CA activity and can be used as pressure-lowering systemic drugs in the treatment of several disorders, including glaucoma and epilepsy [6,7]. However, these inhibitors are known to cause undesirable side effects such as fatigue, paresthesia, gastric and duodenal ulcers, neurological disorders, idiopathic intracranial hypertension, or osteoporosis [8,9]. They inhibit CA isoforms found in many tissues and organs outside the eye. Also, they are primarily used for the treatment of glaucoma [10].

* Corresponding authors.
*E-mail addresses:* tapelzy@yahoo.com (M. Tapera), emin@erciyes.edu.tr (E. Sarıpınar).

https://doi.org/10.1016/j.molliq.2023.123242
Received 21 January 2023; Received in revised form 30 September 2023; Accepted 3 October 2023
Available online 5 October 2023
0167-7322/

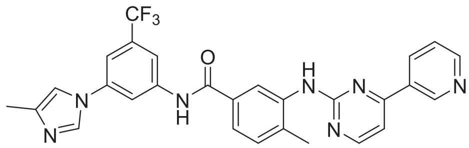

**Nilotinib**

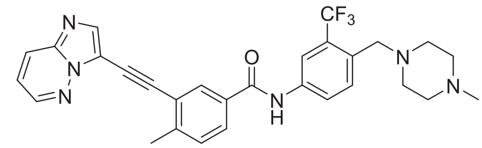

**Ponatinib**

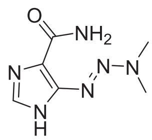

**Dacarbazine**

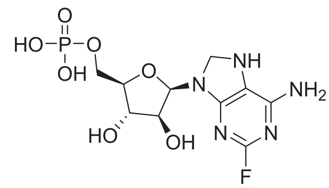

**Fludarabine phosphate**

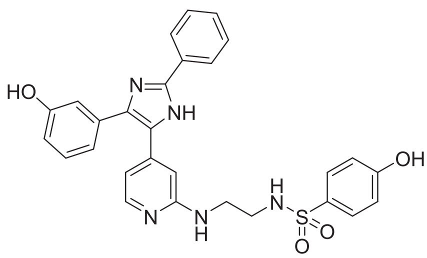

**1**

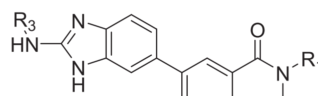

**2**

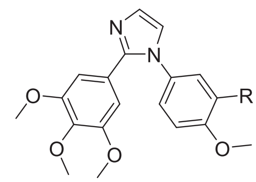

**3**

**Fig. 1.** Commercial drugs and biologically active compounds imidazole moiety.

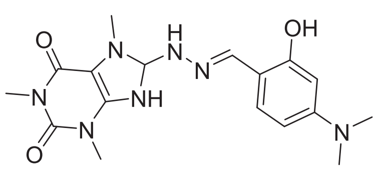

**4**

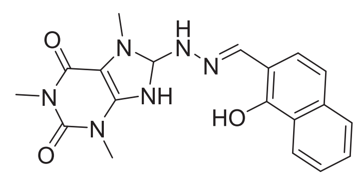

**5**

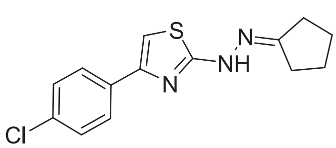

**6**

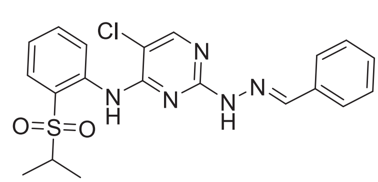

**7**

**Fig. 2.** Hydrazone based hybrid compounds with anticancer activity.

Nitrogen-containing heterocycles, particularly imidazole, are one of the important scaffolds exhibiting a wide range of pharmacological activities, including anticancer [11,12], antiviral [13], antibacterial [14], antitubercular [15], and antiepileptic [16]. This scaffold is found in a copious number of marketed drugs as anticancer agents, such as nilotinib, dacarbazine, ponatinib, and fludarabine phosphate see Fig. 1. In addition, several imidazole-based compounds have revealed anticancer activities through different mechanisms of action, including induction of apoptosis, inhibition of angiogenesis, inhibition of tubulin polymerization, and antiestrogenic activity. The noteworthy bioactivity of compounds carrying an imidazole ring is postulated to be because of its high polarity properties (experimental logP close to zero) [17], due to the presence of two nitrogen atoms, and the capability of the imidazole ring to be a hydrogen bond donor [18], allowing it to interact with molecular targets such as receptors and enzymes [19]. Various imidazole derivatives have been synthesized by linking them to other moieties. Interestingly, a lot of effective anticancer agents have been developed as a result of combining the imidazole ring with other moieties. For instance, in 2021, E.M.H. Ali et al. reported an imidazole-based compound with sulfonamide functionality (**1**) in Fig. 1 with

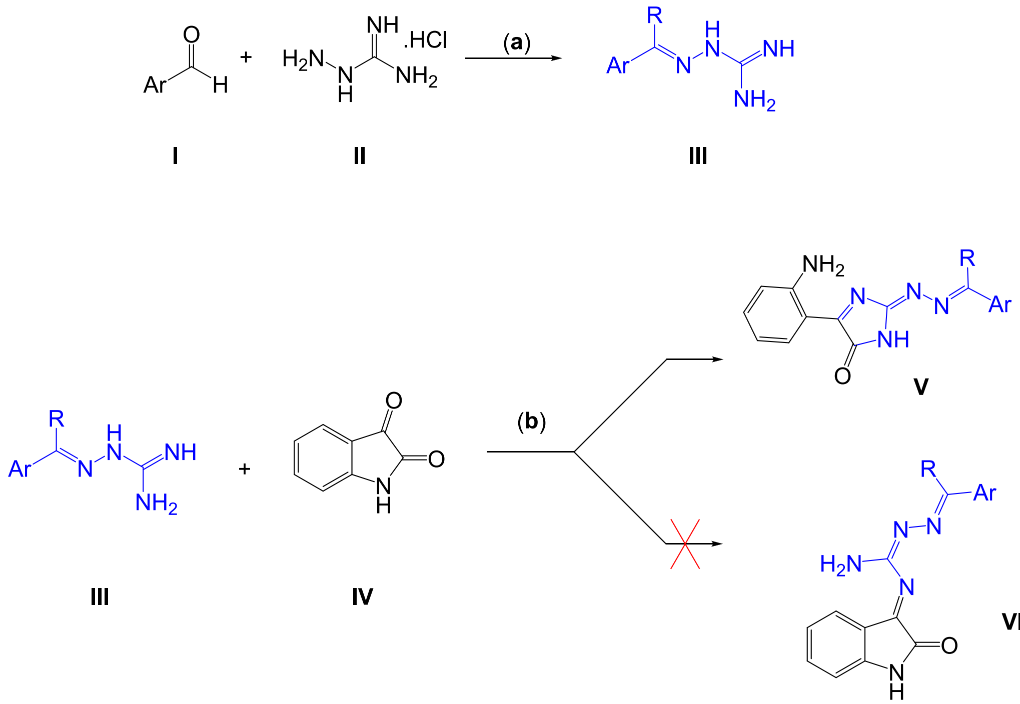


**Scheme 1.** Synthetic route of 5-imidazol-4-one derivatives (**FRB 1–13**). Conditions and reagents: Ethanol, potassium hydroxide, room temperature, 3 h. (b) isatin, Ethanol, reflux 8 h.

potential anticancer activity and an exceptional value of half-maximal inhibitory concentration ($IC_{50}$) of 32 nm. These compounds were investigated using melanoma human cancer cell lines via BRAFV600E kinase inhibition [20]. Not long ago, Fan et al. reported imidazole derivatives connected to a quinazoline group (**2**) in Fig. 1 with potential anti-proliferative activity on a variety of cancerous cells, including the prostate cancer cell line (PC3). These compounds had significant IC50 values between 0.38 and 0.77 μM [21]. Also, Li et al. synthesized 1-substituted-2-aryl imidazoles (**3**), which displayed significant anti-proliferative activities with $IC_{50}$ values in the range of 80–100 nM and selectivity on health cell lines as good as clinically administered drugs [22] (see Fig. 2).

On the other hand, the hydrazone moiety is one of the most extensively used scaffolds in the design and discovery of new lead compounds, particularly in the design of antiproliferative agents [23–25]. Many hydrazone-containing compounds have been found to have potent anticancer activity [14,26]. The anticancer activity of the hydrazone moiety was hypothesized to be suspectable to establish and accommodate hydrogen bonds with molecular targets, and the N═C was also feasible for the addition process of nucleophile groups such as amino –$NH_2$ and thiol -SH in the target molecules, which will enhance its activity [27,28]. For instance, hydrazone derivatives 4 and 5 in Fig. 2 exhibited a significant level of cytotoxicity and exceptional selectivity against cancerous cells over non-cancerous cells [29]. In addition, compound 6 (CPTH2) was discovered to be an apoptosis inducer with dual inhibitory effects on GCN5 and PCAF [30]. Also, Compound 7, a pyrimidine-hydrazone hybrid, exhibited remarkable antiproliferative activity against different cell lines, such as A549, H460, and HT-29, by targeting ALK and ROS1 [31].

Recent studies show that theoretical calculations become very important in many stages, from synthesis and characterization to activity comparison [32]. There are many programs to use for these stages. The most well-known among these programs are Gaussian software [33] and Maestro Schrödinger [34]. The chemical properties of the molecules were examined with the Gaussian software program, which was used to calculate the B3LYP, HF, and M06-2X [35,36]. levels with the 6-31++g (d,p) basis sets. On the other hand, their activities were compared against various proteins using the Maestro Schrödinger program. In order to anticipate the action, response, and transport of synthesized molecules in human metabolism, ADME/T calculations were conducted.

One of the principal strategies for drug discovery is to combine two or more pharmacophoric moieties in a single molecule to obtain potent bioactive molecules with a novel mechanism of action. Consequently, the significant biological activity of compounds with an imidazole ring incorporated into their structure and a hydrazone moiety has inclined us to synthesize molecules that have both of these crucial scaffolds in one molecule. These compounds were designed and synthesized as illustrated in Scheme 1.

## 2. Experiment

### 2.1. Chemistry

Unless otherwise noted, all materials were obtained from commercial sources and used without purification. To determine reaction duration and product purity, thin-layer chromatography (TLC) with fluorescent indicators visible at 254 nm and 365 nm was used. Melting points were obtained using open glass capillaries and were uncorrected. Infrared (IR) spectra were determined via an ATR diamond in the range 4000–700 $cm^{-1}$. H-NMR (400 MHz) spectra and C-NMR (100 MHz) spectra were recorded on a Bruker AM 400 MHz NMR spectrometer with $CDCl_3$ or DMSO-$d_6$ as the solvent. Coupling constants, J, are reported in hertz (Hz). MS spectra were obtained using an Agilent 1200/6530 LC/MS High-Resolution Time of Flight (TOF) instrument.

General Procedure for the synthesis of aminoguanidine derivatives 2-benzylidenehydrazinecarboximidamide derivatives **(III).**

These compounds were synthesized using the modified literature technique [37]. Benzal aldehydes or ketones (I) (0.1 mmol) and aminoguanidine (II) (0.11 mmol) in 15 mL of water were stirred at room temperature for 1 h. The outcome of this mixture formed a suspension, which was then neutralized with excess 2 N NaOH. The precipitate materials were filtered off, washed with water, and dried to afford crystals.

General procedure for the synthesis of synthesis of target compounds

**Table 1**
Structure and physical characteristics of synthesized compounds **FRB**(**1**–**13**).[45].

| Compounds | Structure | Yield% | M.p (°C) | Molecular Weight |
|---|---|---|---|---|
| **FRB-1** | 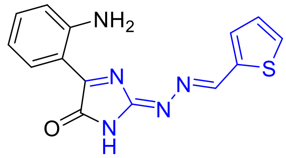 | 77 | 302–304 | 298 |
| **FRB-2** | 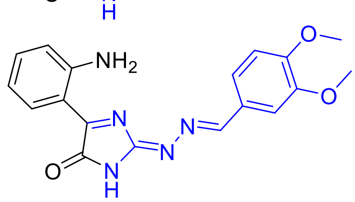 | 89 | 276–278 | 352 |
| **FRB-3** | 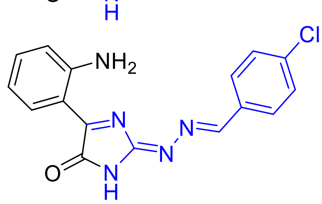 | 88 | 314–316 | 326 |
| **FRB-4** | 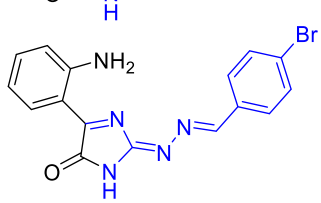 | 69 | 309–311 | 370 |
| **FRB-5** | 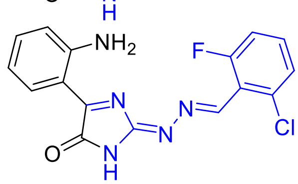 | 67 | 303–305 | 344 |
| **FRB-6** | 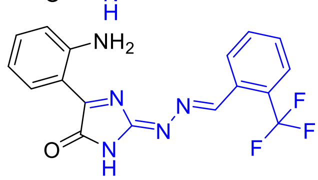 | 59 | 320–322 | 360 |
| **FRB-7** | 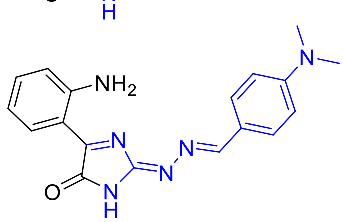 | 77 | 306–308 | 335 |
| **FRB-8** | 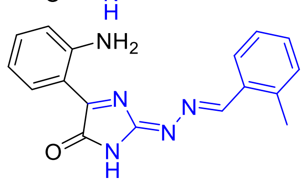 | 89 | 302–304 | 306 |
| **FRB-9** | 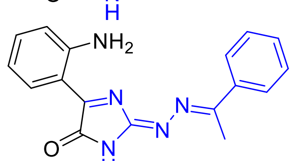 | 88 | 284–286 | 306 |
| **FRB-10** | 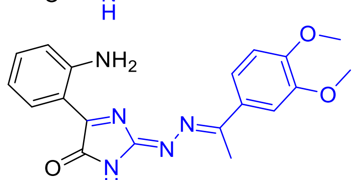 | 87 | 278–280 | 366 |

(*continued on next page*)

**Table 1** (*continued*)

| Compounds | Structure | Yield% | M.p (°C) | Molecular Weight |
|---|---|---|---|---|
| **FRB-11** | 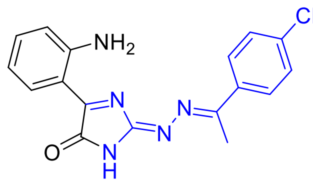 | 76 | 163–165 | 359 |
| **FRB-12** | 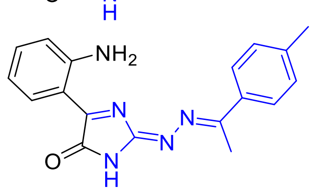 | 66 | 164–166 | 307 |
| **FRB-13** | 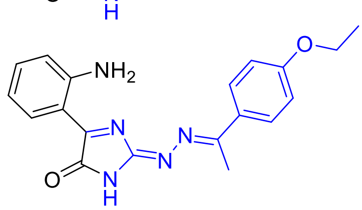 | 90 | 285–287 | 350 |

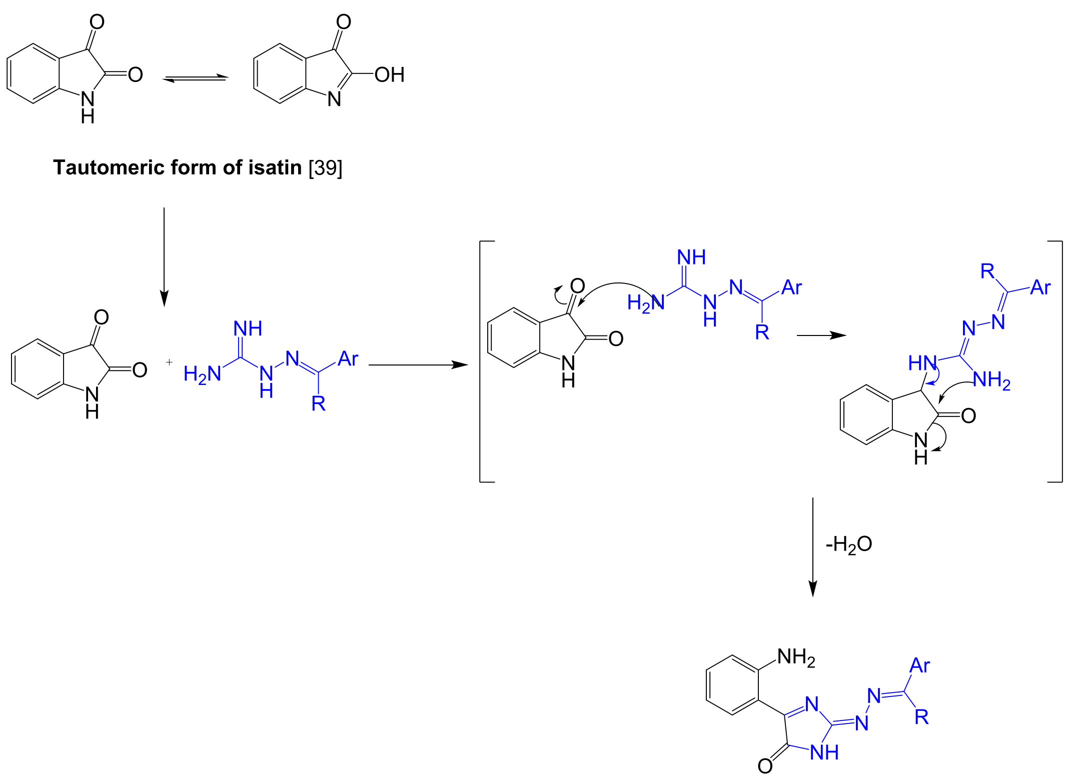


**Scheme 2.** The probable mechanism for the formation of target compounds **FRB (1–13)**.

**FRB (1–13).**

To a boiling solution of guanylhydrazone derivatives (**III**) (0.1 mmol) in 10 mL EtOH was added Indole-2,3-dione (IV) (0.1 mmol) and the mixture was refluxed until total consumption of starting materials (monitored by thin layer chromatography) 8 h. After cooling, the precipitate formed was filtered and recrystallized using the appropriate solvents.

5-(2-Aminophenyl)-2-((thiophen-2-ylmethylene)hydrazono)-2,3-dihydro-4H-imidazol-4-one (**FRB-1**) *Burgundy solid, yield:77 %, TLC:Rf = 0.31 (EA/CH = 4:6) [UV active], Mp 302–304 °C. IR (ATR) 3370.7, 3189.2, 1728.6, 1639.3, 1619.9, 1572.2, 1552.9, 1515.3, 1484.9, 1441.7, 1359.4, 1308.7, 1260.1, 1200.3.* $^{1}H$ *NMR (400 MHz, DMSO) δ 12.16 (s, 1H, NH imidazole), 8.79 (s, 1H, CH), 8.69 (d, J = 8.4 Hz, 1H, Ar-H), 7.93 (s, 2H, Ar-NH*$_2$*), 7.85 (d, J = 4.9 Hz, 1H, Ar-H), 7.71 (s, 1H, Ar-H), 7.38 – 7.27 (m, 1H, Ar-H), 7.26 – 7.17 (m, 1H, Ar-H), 6.88 (d, J = 8.6 Hz, 1H, Ar-H), 6.62 (t, J = 7.5 Hz, 1H, Ar-H).* $^{13}C$ *NMR (101 MHz, DMSO) δ 166.67 (C=O), 163.82 (C2 imidazole), 162.00, 160.76, 154.49, 144.55, 136.29, 132.09, 131.13, 130.82, 129.51, 116.50, 115.30, 111.89. HRMS (EI): [M + H]*$^+$*, found 298.0754.* $C_{14}H_{11}N_5OS$ *requires 298.0756.*

5-(2-aminophenyl)-2-((3,4-dimethoxybenzylidene)hydrazono)-2,3-dihydro-4H-imidazol-4-one (**FRB-2**) *Dark red, yield:89 %, TLC:Rf = 0.38 (EA/CH = 3:7) [UV active], Mp 276–278 °C. IR (ATR) 3375.0, 3187.6,*

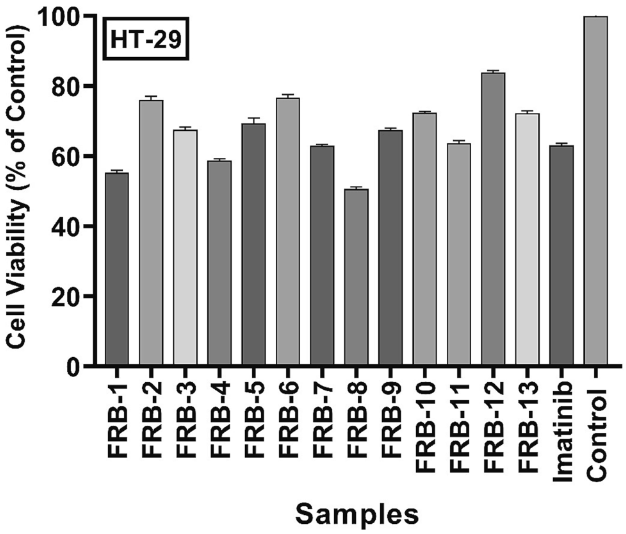


**Fig. 3.** Cytotoxic activities of 5-imidazol-4-one derivatives **FRB (1**–**13)** on HT-29 cell line. FRB-1, FRB-4 and FRB-8 showed the most cytotoxic activity on HT-29 cell line.

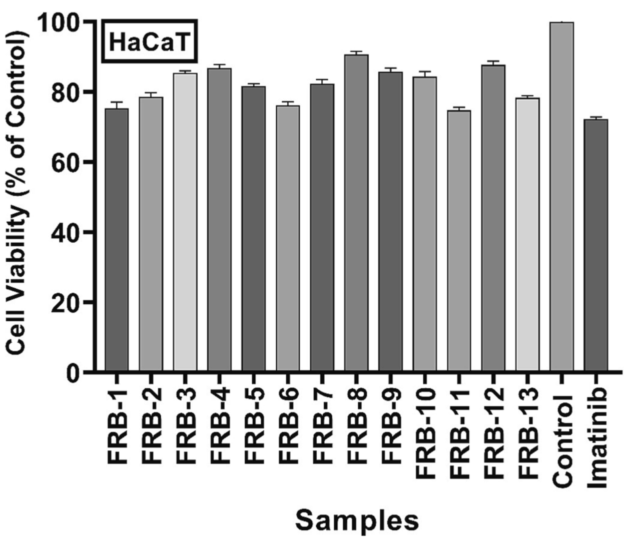


**Fig. 4.** Cytotoxic activities of 5-imidazol-4-one derivatives (FRB1-13) on HaCaT cell line.

*2831.9, 1720.3, 1620.5, 1596.8, 1572.2, 1511.9, 1479.0, 1437.1, 1337.7, 1313.4, 1254.4, 1169.6, 1128.4.* $^{1}$*H NMR (400 MHz, DMSO) δ 12.29 (s, 1H, NH imidazole), 8.71 (d, J = 7.7 Hz, 1H, Ar-H), 8.54 (s, 1H, CH), 7.94 (s, 1H, Ar-*$NH_2$*), 7.83 (s, 1H, Ar-H), 7.43 (d, J = 7.1 Hz, 1H, Ar-H), 7.32 (t, J = 7.1 Hz, 1H, Ar-H), 7.06 (d, J = 8.3 Hz, 1H, Ar-H), 6.88 (d, J = 8.4 Hz, 1H, Ar-H), 6.63 (t, J = 7.6 Hz, 1H, Ar-H), 3.87 (s, 3H,* $OCH_3$*), 3.83 (s, 3H,* $OCH_3$*).* $^{13}$*C NMR (101 MHz, DMSO) δ 166.72 (C═O), 163.64 (C2 imidazole), 161.04, 160.46, 153.28, 152.38, 149.53, 135.10, 131.11, 127.55, 125.43, 116.23, 116.45, 111.40, 110.51, 110.17, 56.12 (d, J = 5.9 Hz,* $OCH_3$*). HRMS (EI):* $[M + H]^+$*, found 352.1404.* $C_{18}H_{17}N_5O_3$ *requires 352.1410.*

5-(2-Aminophenyl)-2-((4-chlorobenzylidene)hydrazono)-2,3-dihydro-4H-imidazol-4-one (**FRB-3**) *Maroon, yield: 79 %, TLC:Rf = 0.26 (EA/CH = 3:7) [UV active], Mp 314–316 °C. IR (ATR) 3347.3, 3185.4, 1727.3, 1647.9, 1620.3, 1599.5, 1519.0, 1485.1, 1438.3, 1311.3, 1257.6, 1157.4, 1079.4, 954.5.* $^{1}$*H NMR (400 MHz, DMSO) δ 12.31 (s, 1H, NH imidazole), 8.79 (d, J = 8.4 Hz, 1H, Ar-H), 8.63 (s, 1H, CH), 8.09 (d, J = 8.3 Hz, 2H, Ar-H), 7.98 (s, 2H, Ar-*$NH_2$*), 7.58 (d, J = 8.1 Hz, 1H, Ar-H),*

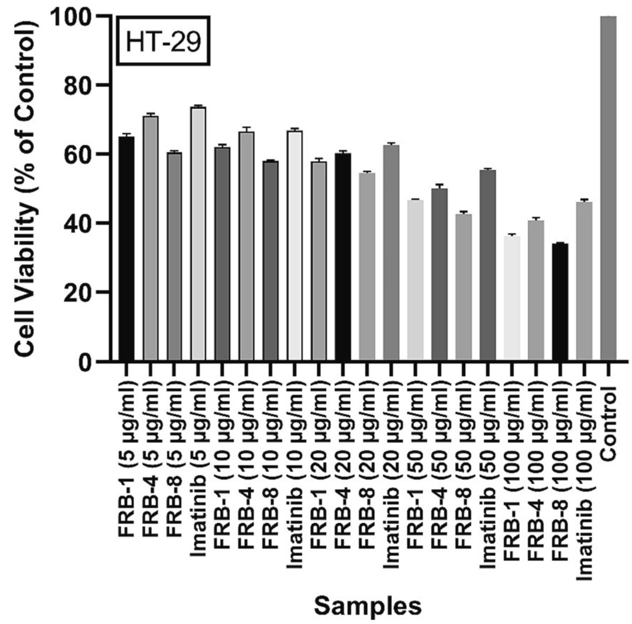


**Fig. 5.** Concentration dependent cell viability results of compounds (**FRB-1**, **FRB-4** and **FRB-8**) in HT-29 cell line.

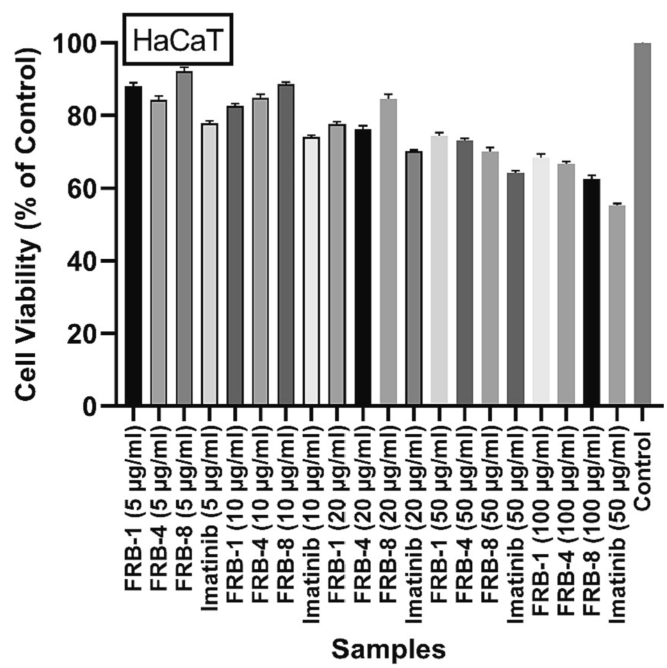


**Fig. 6.** Concentration dependent cell viability results of the synthesized compounds on HaCaT cell line.

**Table 2**
$IC_{50}$ values of **FRB-1**, **FRB-4** and **FRB-8** compounds on HT-29 and HaCaT cells following incubation for 24 h.

| | HT-29 | HaCaT |
|---|---|---|
| | $IC_{50}$ (µg/mL ± SEM) | |
| | 24 h | 24 h |
| **FRB-1** | 36.78 ± 0.17 | ≥100 |
| **FRB-4** | 49.76 ± 0.22 | ≥100 |
| **FRB-8** | 30.84 ± 0.19 | ≥100 |
| **Imatinib** | 57.34 ± 0.25 | ≥100 |

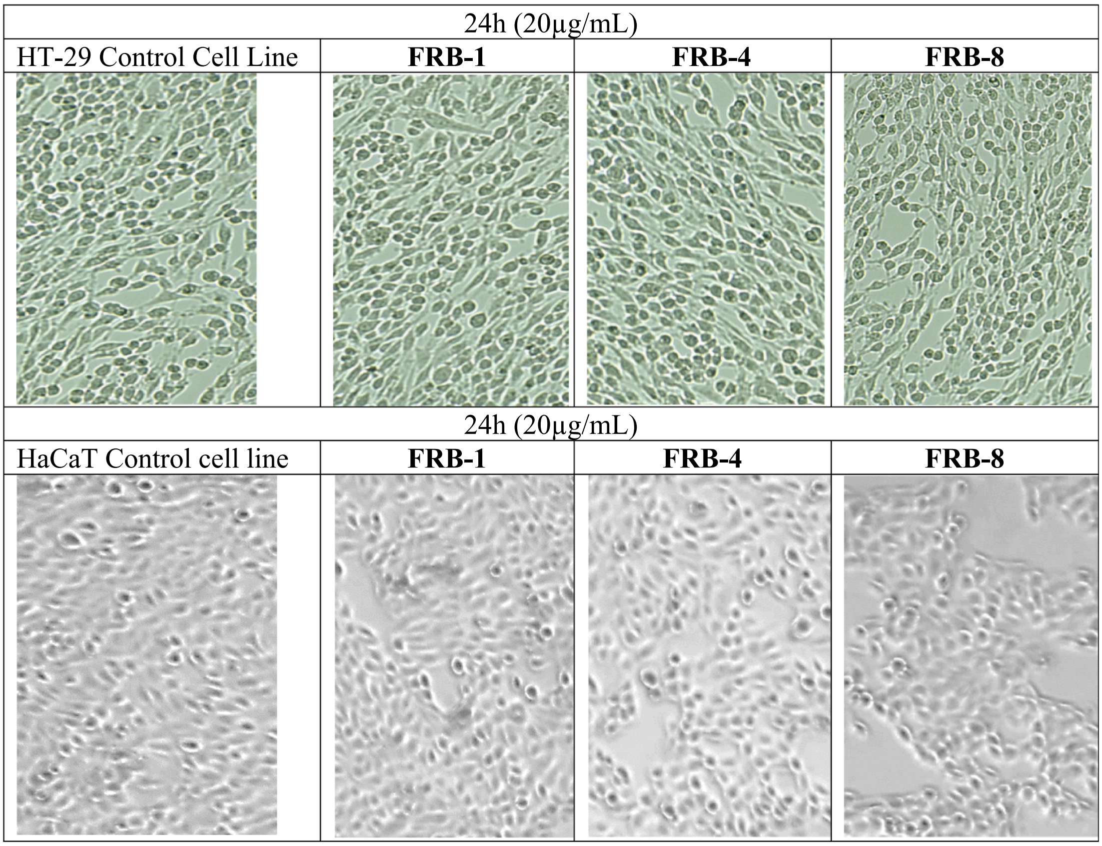


**Fig. 7.** Morphological features of HT-29 and HaCaT cell lines after 24 h of incubation of derivatives **FRB-1**, **FRB-4** and **FRB-8**. The morphological properties of the three components that presented the highest antiproliferative effect against HT-29 cell line are presented in this figure.

*7.42 (t, J = 7.5 Hz, 1H, Ar-H), 6.88 (d, J = 8.5 Hz, 1H, Ar-H), 6.63 (t, J = 7.5 Hz, 1H, Ar-H). $^{13}$C NMR (101 MHz, DMSO) δ 165.66 (C=O), 163.20 (C2 imidazole), 161.45, 158.74, 154.66, 135.48, 136.35, 133.67, 132.55, 132.07, 128.45 (s), 115.70, 115.95, 110.32. HRMS (EI): $[M + H]^+$, found 326.0803. $C_{16}H_{12}ClN_5O$ requires 326.0803.*

5-(2-Aminophenyl)-2-((4-bromobenzylidene)hydrazono)-2,3-dihydro-4H-imidazol-4-one (**FRB-4**) *Maroon, yield: 79 %, TLC:Rf = 0.41 (EA/CH = 4:6) [UV active], Mp 314–316 °C. IR (ATR) 3347.3, 3185.4, 1727.3, 1647.9, 1620.3, 1599.5, 1519.0, 1485.1, 1438.3, 1311.3, 1257.6, 1157.4, 1079.4, 954.5. $^1$H NMR (400 MHz, DMSO) δ 12.30 (s, 1H, NH imidazole), 8.68 (d, J = 8.6 Hz, 1H, Ar-H), 8.65 (s, 1H, CH), 8.09 (d, J = 8.4 Hz, 2H, Ar-H), 7.88 (s, 2H, Ar-$NH_2$), 7.58 (d, J = 8.5 Hz, 1H, Ar-H), 7.44 (t, J = 7.4 Hz, 1H, Ar-H), 6.88 (d, J = 8.3 Hz, 1H, Ar-H), 6.63 (t, J = 7.5 Hz, 1H, Ar-H). $^{13}$C NMR (101 MHz, DMSO) δ 166.76 (C=O), 164.00 (C2 imidazole), 161.39, 159.71, 153.65, 136.47, 135.25, 133.17, 132.85, 132.17, 129.32 (s), 116.73, 115.84, 110.32. HRMS (EI): $[M + H]^+$, found 326.0803. $C_{16}H_{12}ClN_5O$ requires 326.0803.*

5-(2-Aminophenyl)-2-((2-chloro-6-fluorobenzylidene)hydrazono)-2,3-dihydro-4H-imidazol-4-one (**FRB-5**) *Burgundy solid, yield: 67 %, TLC:Rf = 0.38 (EA/CH = 2:8) [UV active], Mp 303–305 °C. IR (ATR) 3370.7, 3245.7, 2918.1, 1739.9, 1643.1, 1623.8, 1524.9, 1462.6, 1438.9, 1312.1, 1262.6, 1159.4, 957.4. $^1$H NMR (400 MHz, DMSO) δ 12.04 (s, 1H, NH imidazole), 8.74 (s, 1H, CH), 8.65 (t, J = 9.5 Hz, 1H, Ar-H), 7.99 (s, 2H, Ar-$NH_2$), 7.63 – 7.52 (m, 1H, Ar-H), 7.47 (d, J = 8.1 Hz, 1H, Ar-H), 7.39 (t, J = 9.2 Hz, 1H, Ar-H), 7.33 (d, J = 7.6 Hz, 1H, Ar-H), 6.88 (d, J = 8.4 Hz, 1H, Ar-H), 6.63 (t, J = 7.8 Hz, 1H, Ar-H). $^{13}$C NMR (101 MHz, DMSO) δ 167.47 (C=O), 166.84 (C2 imidazole), 161.84, 156.45, 154.83, 135.62, 135.76, 134.51, 133.41, 134.12, 131.17, 130.67, 127.14, 116.83, 116.12, 110.26. HRMS (EI): $[M + H]^+$, found 344.0708. $C_{16}H_{11}ClFN_5O$ requires 344.0710.*

5-(2-Aminophenyl)-2-((2-(trifluoromethyl)benzylidene)hydrazono)-2,3-dihydro-4H-imidazol-4-one (**FRB-6**) *Red solid, yield: 59 %, TLC:Rf = 0.23 (EA/CH = 1:9) [UV active], M.p 320–322 °C. IR (ATR) 3379.3, 3185.3, 1723.3, 1644.3, 1621.6, 1521.3, 1481.9, 1439.1, 1346.5, 1164.0, 1104.1, 1034.7, 953.0. $^1$H NMR (400 MHz, DMSO) δ 12.45 (s, 1H, NH imidazole), 8.93 (s, 1H, Ar-H), 8.74 (s, 1H, =CH), 8.73 (d, J = 8.5 Hz, 1H, Ar-H), 8.45 (d, J = 7.3 Hz, 1H, Ar-H), 8.32 (d, J = 8.5 Hz, 1H, Ar-H), 8.01 (s, 2H, Ar-$NH_2$), 7.79 (t, J = 8.2 Hz, 1H, Ar-H), 7.13 (t, J = 7.3 Hz, 1H, Ar-H), 6.89 (d, J = 8.7 Hz, 1H, Ar-H), 6.63 (t, J = 7.5 Hz, 1H, Ar-H). $^{13}$C NMR (101 MHz, DMSO) δ 166.73 (C=O), 164.24 (C2 imidazole), 162.01, 160.47, 154.17, 152.16, 149.54, 137.33, 132.19, 127.67, 125.32, 116.55, 115.88, 111.66, 110.46, 110.15. HRMS (EI): $[M + H]^+$, found 360.1066. $C_{17}H_{12}F_3N_5O$ requires 360.0994.*

5-(2-Aminophenyl)-2-((4-(dimethylamino)benzylidene)hydrazono)-2,3-dihydro-4H-imidazol-4-one (**FRB-7**) *Black solid, yield: 77 %, TLC:Rf = 0.42 (EA/CH = 4:6) [UV active], M.p 306–308 °C. IR (ATR) 3375.0, 1712.8, 1640.1, 1606.5, 1568.4, 1511.2, 1434.0, 1305.5, 1154.6, 1049.9, 943.8. $^1$H NMR (400 MHz, DMSO) δ 12.13 (s, 1H, NH), 8.71 (d, J = 7.7 Hz, 1H, Ar-H), 8.46 (s, 1H, N = CH), 7.88 (s, 4H, Ar-$NH_2$, Ar-H), 7.30 (s, 1H, Ar-H), 6.87 (d, J = 8.3 Hz, 1H, Ar-H), 6.77 (d, J = 7.6 Hz, 2H, Ar-H), 6.62 (s, 1H, Ar-H), 3.03 (s, 6H, $CH_3$). $^{13}$C NMR (101 MHz, DMSO) δ 166.67 (C=O), 164.39 (C2 imidazole), 161.82, 160.42, 154.73, 153.54, 136.23, 133.74, 134.33, 128.83, 123.79, 122.16, 116.36, 115.78, 112.33, 111.42, 56.30 (2$CH_3$). HRMS (EI): $[M + H]^+$, found 335.1614. $C_{18}H_{18}N_6O$ requires 335.1542.*

5-(2-Aminophenyl)-2-((2-methylbenzylidene)hydrazono)-2,3-dihydro-4H-imidazol-4-one (**FRB-8**) *Dark-red solid, yield: 89 %, TLC:Rf = 0.38 (EA/CH = 2:8) [UV active], Mp 302–304 °C. IR (ATR) 3362.1, 3187.0, 1722.3, 1644.3, 1619.9, 1551.5, 1519.2, 1480.1,1438.3, 1368.8, 1310.2, 1255.2, 1202.4, 1159.8. $^1$H NMR (400 MHz, DMSO) δ 12.22 (s, 1H, NH imidazole), 9.86 (s, 1H, CH), 8.70 (d, J = 8.5 Hz, 1H, Ar-H), 8.34 (d, J = 7.2 Hz, 1H, Ar-H), 7.95 (s, 2H, Ar-$NH_2$), 7.39 (t, J = 7.5 Hz, 1H, Ar-H), 7.31 (dd, J = 16.8, 7.6 Hz, 3H, Ar-H), 6.89 (d, J = 8.5 Hz, 1H, Ar-H), 6.63 (t, J = 7.6 Hz, 1H, Ar-H), 2.50 (s, 3H, $CH_3$). $^{13}$C NMR (101 MHz,*

**Table 3**
Results of the enzyme inhibition of carbonic anhydrase I and II isoenzymes by synthesized compounds FRB(1–13).

| Compounds | $IC_{50}$ (nM) | | | | Ki (nM) | |
|---|---|---|---|---|---|---|
| | hCA I | $r^2$ | hCA II | $r^2$ | hCA I | hCA II |
| FRB-1 | 0.7647 | 0.9427 | 0.1904 | 0.9975 | 739.12 ± 111.35 | 146.56 ± 61.39 |
| FRB-2 | 1.1917 | 0.9180 | 1.1605 | 0.9507 | 94.14 ± 9.99 | 314.36 ± 54.07 |
| FRB-3 | 1.8570 | 0.8688 | 1.4382 | 0.9518 | 221.85 ± 112.81 | 179.57 ± 93.68 |
| FRB-4 | 1.4928 | 0.9910 | 1.0574 | 0.9940 | 301.53 ± 190.95 | 181.34 ± 39.36 |
| FRB-5 | 1.0984 | 0.9950 | 1.2112 | 0.9893 | 284.37 ± 89.90 | 202.27 ± 100.99 |
| FRB-6 | 1.3543 | 0.9958 | 1.5508 | 0.9368 | 238.45 ± 113.98 | 210.13 ± 93.05 |
| FRB-7 | 0.5940 | 0.9934 | 1.3588 | 0.9722 | 639.48 ± 214.63 | 100.89 ± 58.35 |
| FRB-8 | 1.0612 | 0.9723 | 0.9025 | 0.9133 | 6.49 ± 1.010 | 156.21 ± 60.82 |
| FRB-9 | 0.8467 | 0.9370 | 1.3509 | 0.9455 | 251.47 ± 176.64 | 89.58 ± 21.24 |
| FRB-10 | 0.7932 | 0.9851 | 0.7937 | 0.8334 | 182.66 ± 92.28 | 64.53 ± 19.44 |
| FRB-11 | 0.9751 | 0.9723 | 0.6813 | 0.9953 | 65.16 ± 14.65 | 185.89 ± 64.99 |
| FRB-12 | 1.8203 | 0.9639 | 1.8280 | 0.9984 | 108.87 ± 35.39 | 146.56 ± 61.39 |
| FRB-13 | 0.6344 | 0.8081 | 0.6448 | 0.8183 | 79.05 ± 44.51 | 314.37 ± 54.78 |
| AZA | 12.62 | 0.9712 | 19.81 | 0.9706 | 271.15 ± 74.62 | 113.07 ± 20.98 |

*AZA (acetazolamide) was used as a positive control for human carbonic anhydrase I and II isoforms (hCA I and II).

*DMSO) δ 166.66 (C=O), 163.84 (C2 imidazole), 161.03, 160.65, 153.59, 142.15, 134.29, 132.09, 131.23, 127.32, 129.51, 117.36, 115.88 (s, J = 15.7 Hz), 110.39, 21.69. HRMS (EI): [M + H]$^+$, found 306.1349. $C_{17}H_{15}N_5O$ requires 306.1352.*

5-(2-Aminophenyl)-2-((1-phenylethylidene)hydrazono)-2,3-dihydro-4H-imidazol-4-one (**FRB-9**).

*Black solid, yield: 88 %, TLC:Rf = 0.31 (EA/CH = 3:7) [UV active], Mp 284–286 °C. IR (ATR) 3409.5, 3375.0, 3168.1, 1724.5, 1615.2, 1548.8, 1514.5, 1484.2, 1439.9, 1364.7, 1309.3, 1253.5, 1198.1, 1152.1. $^1$H NMR (400 MHz, DMSO) δ 12.14 (s, 1H, NH imidazole), 8.70 (d, J = 8.5 Hz, 1H, Ar-H), 8.18 (d, J = 7.4 Hz, 2H), 7.94 (s, 2H, Ar-NH$_2$), 7.47 (t, J = 6.5 Hz, 3H, Ar-H), 7.32 (d, J = 8.4 Hz, 1H, Ar-H), 6.88 (d, J = 8.2 Hz, 1H, Ar-H), 6.64 (d, J = 7.9 Hz, 1H, Ar-H), 2.50 (s, 3H, CH$_3$). $^{13}$C NMR (101 MHz, DMSO) δ 166.88 (C=O), 165.29 (C2 imidazole), 163.3, 158.7, 153.35, 137.8, 135.0, 131.13, 130.97, 128.69 (s), 128.03, 116.63, 115.87, 110.41, 14.89 (CH$_3$). HRMS (EI): [M + H]$^+$, found 306.1349. $C_{17}H_{15}N_5O$ requires 306.1349.*

5-(2-Aminophenyl)-2-((1-(3,4-dimethoxyphenyl)ethylidene)hydrazono)-2,3-dihydro-4H-imidazol-4-one (**FRB-10**) *Dark-brown, yield: 87 %, TLC:Rf = 0.28 (EA/CH = 2:8) [UV active], Mp 278–280 °C. IR (ATR) 3383.8, 3174.6, 1720.0, 1618.9, 1543.6, 1514.7, 1483.3, 1445.6, 1360.6, 1306.1, 1257.4, 1221.6, 1160.9, 1134.2, 1065.1. $^1$H NMR (400 MHz, DMSO) δ 12.16 (s, 1H, NH imidazole), 8.71 (d, J = 8.3 Hz, 1H, Ar-H), 7.91 (s, 2H, Ar-NH$_2$), 7.86 (d, J = 2.0 Hz, 1H, Ar-H), 7.59 (dd, J = 8.5, 2.0 Hz, 1H, Ar-H), 7.31 (t, J = 7.7 Hz, 1H, Ar-H), 7.00 (d, J = 8.5 Hz, 1H, Ar-H), 6.88 (d, J = 8.4 Hz, 1H, Ar-H), 6.69 – 6.57 (m, 1H, Ar-H), 3.88 (s, 3H, OCH$_3$), 3.82 (s, 3H, OCH$_3$). $^{13}$C NMR (101 MHz, DMSO) δ 166.96 (C=O)), 165.41 (C2 imidazole), 163.15, 157.21, 152.71, 151.78,*

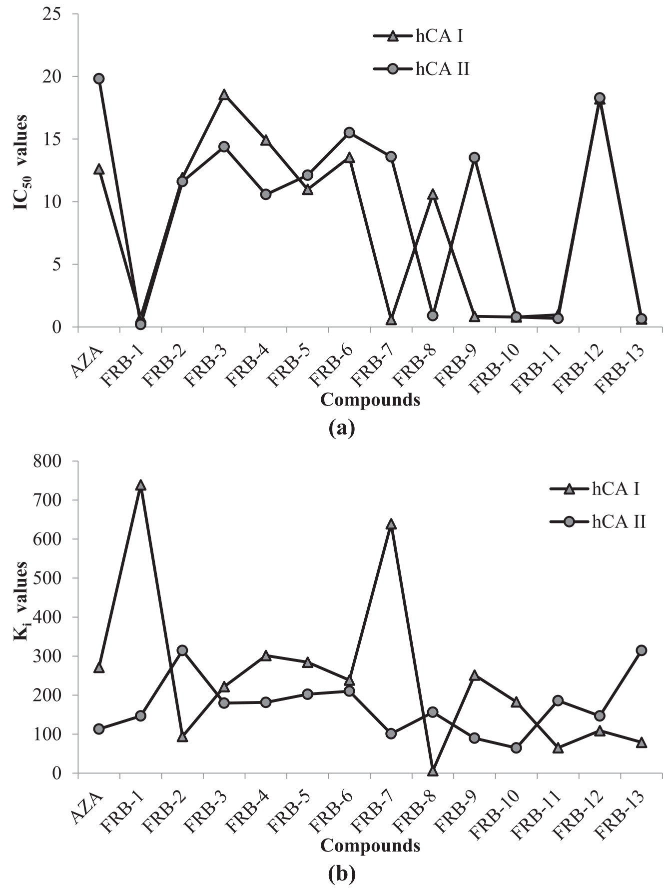


**Fig. 8.** $K_i$ and $IC_{50}$ values for hCA I and hCA II isoenzymes.

*144.98, 132.93, 133.10, 130.51, 122.97, 116.19, 115.81, 112.25, 110.73, 110.50, 56.31 (OCH$_3$), 56.01 (OCH$_3$), 14.78 (CH$_3$). HRMS (EI): [M + H]$^+$, found 366.1560. $C_{19}H_{19}N_5O_3$ requires 366.1562.*

5-(2-Aminophenyl)-2-((1-(4-chlorophenyl)ethylidene)hydrazono)-2,3-dihydro-4H-imidazol-4-one (**FRB-11**) *Black solid, yield: 82 %, TLC: Rf = 0.21 (EA/CH = 4:6) [UV active], Mp 272–274 °C. IR (ATR) 3392.2, 3175.3, 1721.4, 1618.8 1547.3, 1518.9, 1481.5, 1398.1, 1357.2, 1311.4, 1255.3, 1200.3, 1161.9, 1088.7, 1008.9, 943.2. $^1$H NMR (400 MHz, DMSO) δ 12.30 (s, 1H, NH imidazole), 8.40 (d, J = 8.8 Hz, 1H, CH), 8.22 (d, J = 8.6 Hz, 2H, Ar-H), 7.97 (s, 2H, Ar-NH$_2$), 7.51 (d, J = 8.2 Hz, 2H, Ar-H), 7.31 (t, J = 7.2 Hz, 1H, Ar-H), 6.89 (d, J = 8.4 Hz, 1H, Ar-H), 6.63 (t, J = 7.5 Hz, 1H, Ar-H), 2.50 (s, 3H, CH$_3$). $^{13}$C NMR (101 MHz, DMSO) δ 166.93 (C=O), 164.26 (C2 imidazole), 163.44, 159.13, 153.46, 136.73, 135.74, 135.14, 131.13, 129.84, 128.69, 116.66, 115.88, 110.37, 14.75 (CH$_3$). HRMS (EI): [M + H]$^+$, found 340.0949. $C_{17}H_{14}ClN_5O$ requires 340.0949.*

5-(2-Aminophenyl)-2-((1-(p-tolyl)ethylidene)hydrazono)-2,3-dihydro-4H-imidazol-4-one (**FRB-12)** *Brown solid, yield: 91 %, TLC:Rf = 0.42 (EA/CH = 4:6) [UV active], Mp 305–307 °C. IR (ATR) 3385.2, 3173.0, 2918.1, 1719.6, 1638.9, 1614.9, 1547.2, 1479.0, 1436.4, 1355.9, 1311.6, 1202.4, 1161.8, 1019.7. $^1$H NMR (400 MHz, DMSO) δ 12.14 (s, 1H, NH imidazole), 8.70 (d, J = 8.3 Hz, 1H, Ar-H), 8.08 (d, J = 8.2 Hz, 2H, Ar-H), 7.92 (s, 2H, Ar-NH$_2$), 7.35 – 7.28 (m, 2H, Ar-H), 7.26 (d, J = 8.0 Hz, 1H, Ar-H), 6.88 (d, J = 8.4 Hz, 1H, Ar-H), 6.63 (dd, J = 8.1, 7.0 Hz, 1H, Ar-H), 2.48 (s, 3H, CH$_3$), 2.36 (s, 3H, CH$_3$). $^{13}$C NMR (101 MHz, DMSO) δ 166.85 (C=O), 165.34, 163.27, 158.61, 153.28, 140.89, 135.19, 135.02, 131.11, 129.31, 128.05, 116.61, 115.85, 110.45, 21.47 (CH$_3$), 14.77 (CH$_3$). HRMS (EI): [M + H]$^+$, found 320.1505. $C_{18}H_{17}N_5O$ requires 320.1505.*

5-(2-aminophenyl)-2-((1-(4-ethoxyphenyl)ethylidene)hydrazono)-2,3-dihydro-4H-imidazol-4-one (**FRB-13**) *Burgundy solid, yield: 90 %,*

**Table 4**
The calculated quantum chemical parameters of molecules.

| | $E_{HOMO}$ | $E_{LUMO}$ | I | A | ΔE | η | μ | χ | Pİ | ω | ε | dipol | Energy |
|---|---|---|---|---|---|---|---|---|---|---|---|---|---|
| **B3LYP/SDD LEVEL** | | | | | | | | | | | | | |
| **FRB 1** | −5.7169 | −3.1735 | 5.7169 | 3.1735 | 2.5434 | 1.2717 | 0.7864 | 4.4452 | −4.4452 | 7.7691 | 0.1287 | 0.1566 | −35024.7204 |
| **FRB 2** | −5.7079 | −3.1133 | 5.7079 | 3.1133 | 2.5946 | 1.2973 | 0.7708 | 4.4106 | −4.4106 | 7.4975 | 0.1334 | 2.6923 | −30389.4717 |
| **FRB 3** | −5.8608 | −3.2760 | 5.8608 | 3.2760 | 2.5848 | 1.2924 | 0.7737 | 4.5684 | −4.5684 | 8.0742 | 0.1239 | 2.3748 | −38802.1479 |
| **FRB 4** | −5.8630 | −3.2817 | 5.8630 | 3.2817 | 2.5813 | 1.2906 | 0.7748 | 4.5724 | −4.5724 | 8.0992 | 0.1235 | 2.3574 | −96260.3556 |
| **FRB 5** | −5.8464 | −3.1884 | 5.8464 | 3.1884 | 2.6580 | 1.3290 | 0.7524 | 4.5174 | −4.5174 | 7.6774 | 0.1303 | 1.5154 | −41502.6094 |
| **FRB 6** | −5.9441 | −3.3764 | 5.9441 | 3.3764 | 2.5677 | 1.2838 | 0.7789 | 4.6603 | −4.6603 | 8.4582 | 0.1182 | 3.7817 | −35467.2610 |
| **FRB 7** | −5.3313 | −2.8866 | 5.3313 | 2.8866 | 2.4447 | 1.2223 | 0.8181 | 4.1090 | −4.1090 | 6.9062 | 0.1448 | 4.7403 | −29939.5960 |
| **FRB 8** | −5.7563 | −3.1661 | 5.7563 | 3.1661 | 2.5903 | 1.2951 | 0.7721 | 4.4612 | −4.4612 | 7.6835 | 0.1301 | 0.3798 | −27364.7230 |
| **FRB 9** | −5.7079 | −3.0365 | 5.7079 | 3.0365 | 2.6714 | 1.3357 | 0.7487 | 4.3722 | −4.3722 | 7.1560 | 0.1397 | 0.7461 | −27364.8016 |
| **FRB 10** | −5.6573 | −3.0727 | 5.6573 | 3.0727 | 2.5846 | 1.2923 | 0.7738 | 4.3650 | −4.3650 | 7.3720 | 0.1356 | 2.6187 | −32526.8559 |
| **FRB 11** | −5.8608 | −3.2760 | 5.8608 | 3.2760 | 2.5848 | 1.2924 | 0.7737 | 4.5684 | −4.5684 | 8.0742 | 0.1239 | 2.3747 | −38802.1479 |
| **FRB 12** | −5.7256 | −3.1160 | 5.7256 | 3.1160 | 2.6096 | 1.3048 | 0.7664 | 4.4208 | −4.4208 | 7.4891 | 0.1335 | 0.6631 | −27364.8918 |
| **FRB 13** | −5.6557 | −3.0692 | 5.6557 | 3.0692 | 2.5865 | 1.2932 | 0.7733 | 4.3624 | −4.3624 | 7.3578 | 0.1359 | 1.7874 | −29411.3308 |
| **HF/6–31 g LEVEL** | | | | | | | | | | | | | |
| **FRB 1** | −8.1921 | 0.6286 | 8.1921 | −0.6286 | 8.8206 | 4.4103 | 0.2267 | 3.7817 | −3.7817 | 1.6214 | 0.6168 | 1.0082 | −34857.5609 |
| **FRB 2** | −8.1738 | 0.6656 | 8.1738 | −0.6656 | 8.8394 | 4.4197 | 0.2263 | 3.7541 | −3.7541 | 1.5944 | 0.6272 | 2.6838 | −30207.0570 |
| **FRB 3** | −8.3091 | 0.5083 | 8.3091 | −0.5083 | 8.8174 | 4.4087 | 0.2268 | 3.9004 | −3.9004 | 1.7253 | 0.5796 | 1.8253 | −38620.6060 |
| **FRB 4** | −8.3110 | 0.4912 | 8.3110 | −0.4912 | 8.8021 | 4.4011 | 0.2272 | 3.9099 | −3.9099 | 1.7368 | 0.5758 | 1.9135 | −96048.8506 |
| **FRB 5** | −8.2761 | 0.6705 | 8.2761 | −0.6705 | 8.9466 | 4.4733 | 0.2235 | 3.8028 | −3.8028 | 1.6164 | 0.6187 | 1.4154 | −41310.5856 |
| **FRB 6** | −8.3319 | 0.5608 | 8.3319 | −0.5608 | 8.8928 | 4.4464 | 0.2249 | 3.8855 | −3.8855 | 1.6977 | 0.5890 | 2.8019 | −35265.7643 |
| **FRB 7** | −7.5681 | 0.8455 | 7.5681 | −0.8455 | 8.4136 | 4.2068 | 0.2377 | 3.3613 | −3.3613 | 1.3429 | 0.7447 | 3.6274 | −29752.5815 |
| **FRB 8** | −8.2233 | 0.7067 | 8.2233 | −0.7067 | 8.9300 | 4.4650 | 0.2240 | 3.7583 | −3.7583 | 1.5817 | 0.6322 | 0.7872 | −27194.4278 |
| **FRB 9** | −8.1972 | 0.8534 | 8.1972 | −0.8534 | 9.0506 | 4.5253 | 0.2210 | 3.6719 | −3.6719 | 1.4897 | 0.6713 | 1.0070 | −27194.5782 |
| **FRB 10** | −8.1006 | 0.7064 | 8.1006 | −0.7064 | 8.8070 | 4.4035 | 0.2271 | 3.6971 | −3.6971 | 1.5520 | 0.6443 | 2.4208 | −32329.1256 |
| **FRB 11** | −8.3091 | 0.5083 | 8.3091 | −0.5083 | 8.8174 | 4.4087 | 0.2268 | 3.9004 | −3.9004 | 1.7253 | 0.5796 | 1.8249 | −38620.6060 |
| **FRB 12** | −8.1858 | 0.6914 | 8.1858 | −0.6914 | 8.8772 | 4.4386 | 0.2253 | 3.7472 | −3.7472 | 1.5817 | 0.6322 | 1.2473 | −27194.6409 |
| **FRB 13** | −8.1036 | 0.7192 | 8.1036 | −0.7192 | 8.8228 | 4.4114 | 0.2267 | 3.6922 | −3.6922 | 1.5451 | 0.6472 | 1.7644 | −29231.1479 |
| **M062X/6-31 g LEVEL** | | | | | | | | | | | | | |
| **FRB 1** | −7.0304 | −2.3260 | 7.0304 | 2.3260 | 4.7043 | 2.3522 | 0.4251 | 4.6782 | −4.6782 | 4.6522 | 0.2150 | 0.6801 | −35013.5953 |
| **FRB 2** | −7.0337 | −2.2757 | 7.0337 | 2.2757 | 4.7579 | 2.3790 | 0.4203 | 4.6547 | −4.6547 | 4.5537 | 0.2196 | 2.5290 | −30376.9058 |
| **FRB 3** | −7.1362 | −2.4338 | 7.1362 | 2.4338 | 4.7024 | 2.3512 | 0.4253 | 4.7850 | −4.7850 | 4.8691 | 0.2054 | 1.9154 | −38790.2104 |
| **FRB 4** | −7.1324 | −2.4422 | 7.1324 | 2.4422 | 4.6902 | 2.3451 | 0.4264 | 4.7873 | −4.7873 | 4.8865 | 0.2046 | 1.9716 | −96251.2333 |
| **FRB 5** | −7.1120 | −2.3054 | 7.1120 | 2.3054 | 4.8067 | 2.4033 | 0.4161 | 4.7087 | −4.7087 | 4.6127 | 0.2168 | 1.2779 | −41489.9861 |
| **FRB 6** | −7.1746 | −2.4343 | 7.1746 | 2.4343 | 4.7403 | 2.3701 | 0.4219 | 4.8045 | −4.8045 | 4.8696 | 0.2054 | 2.9085 | −35453.2448 |
| **FRB 7** | −6.5822 | −2.0722 | 6.5822 | 2.0722 | 4.5101 | 2.2550 | 0.4435 | 4.3272 | −4.3272 | 4.1517 | 0.2409 | 4.5686 | −29926.6036 |
| **FRB 8** | −7.0644 | −2.2692 | 7.0644 | 2.2692 | 4.7952 | 2.3976 | 0.4171 | 4.6668 | −4.6668 | 4.5418 | 0.2202 | 0.8289 | −27352.8956 |
| **FRB 9** | −7.0277 | −2.1560 | 7.0277 | 2.1560 | 4.8717 | 2.4358 | 0.4105 | 4.5918 | −4.5918 | 4.3280 | 0.2311 | 1.2275 | −27353.0252 |
| **FRB 10** | −7.0013 | −2.2504 | 7.0013 | 2.2504 | 4.7509 | 2.3754 | 0.4210 | 4.6258 | −4.6258 | 4.5041 | 0.2220 | 2.4347 | −32513.0696 |
| **FRB 11** | −7.1362 | −2.4338 | 7.1362 | 2.4338 | 4.7024 | 2.3512 | 0.4253 | 4.7850 | −4.7850 | 4.8691 | 0.2054 | 1.9154 | −38790.2104 |
| **FRB 12** | −7.0394 | −2.2741 | 7.0394 | 2.2741 | 4.7653 | 2.3826 | 0.4197 | 4.6567 | −4.6567 | 4.5506 | 0.2198 | 1.0469 | −27353.0176 |
| **FRB 13** | −6.9991 | −2.2422 | 6.9991 | 2.2422 | 4.7569 | 2.3784 | 0.4204 | 4.6207 | −4.6207 | 4.4884 | 0.2228 | 1.6225 | −29398.7983 |

*TLC:Rf = 0.43 (EA/CH = 4:6) [UV active], Mp 285–287 °C. IR (ATR) 3387.9, 3175.8, 2982.8, 1717.1, 16017.8, 1564.4, 1521.0, 1443.8, 1391.6, 1311.7, 1253.3, 1206.7, 1161.7, 1118.7, 938.53. $^{1}H$ NMR (400 MHz, DMSO) δ 12.13 (s, 1H, NH imidazole), 8.70 (d, J = 8.1 Hz, 1H, Ar-H), 8.14 (d, J = 8.8 Hz, 2H, Ar-H), 7.90 (s, 2H, Ar-$NH_2$), 7.30 (t, J = 7.7 Hz, 1H, Ar-H), 6.97 (d, J = 8.8 Hz, 2H, Ar-H), 6.87 (d, J = 8.3 Hz, 1H, Ar-H), 6.62 (t, J = 7.7 Hz, 1H, Ar-H), 4.09 (dd, J = 13.9, 6.9 Hz, 2H, $OCH_2$), 2.47 (s, 3H, $CH_3$), 1.34 (t, J = 6.9 Hz, 3H, $CH_3$. $^{13}C$ NMR (101 MHz, DMSO) δ 166.78 (C=O), 165.16 (C2 imidazole), 163.12, 161.07, 158.41, 153.15, 134.99, 131.07, 129.86, 116.60, 115.90, 114.44, 110.48, 63.74 ($OCH_2$), 15.00 ($CH_3$), 14.61 ($CH_3$). HRMS (EI): $[M + H]^+$, found 350.1611 $C_{19}H_{19}N_5O_2$ requires 350.1611.*

## 2.2. Cell culture

In the cell culture study, HT-29 and HaCaT were obtained from ATCC. Fetal bovine serum (FBS) and Dulbecco's modified Eagle's medium (DMEM) were procured from Merck Millipore. Phosphate buffered saline (PBS) and penicillin–streptomycin-L-glutamine solution were bought from Sigma-Aldrich. In cytotoxicity investigations, the Roche Diagnostic XTT assay kit was used. HT-29 and HaCaT cell lines were seeded in DMEM, including FBS (10 %), penicillin (100 IU/mL), L-glutamine (1 %), and streptomycin (10 mg/mL). Then well plates with cells were incubated in an incubator (5 % CO2 and 37 °C). The cytotoxic activity assay was carried out when cells reached 80–90 % confluence.

## 2.3. Cytotoxicity assay

The XTT test was used to assess the cytotoxic effects of synthetic substances on the HT-29 and HaCaT cell lines. Initially, cells were seeded in 96-well plates, including 100 μL of DMEM (10 % FBS), and incubated overnight. For the cytotoxicity experiment, substances were dissolved in DMSO. The compounds were pipetted into DMEM to homogenize them before being administered to each well at a concentration of 20 g/ml. The control group also received the same quantity of DMSO. The compounds were pipetted into DMEM to homogenize them before being administered to each well at a concentration of 20 g/ml. The control group also received the same quantity of DMSO. A microplate ELISA reader was used to measure the absorbance of XTT-formazan at 450 nm [38]. Compounds' cell viability was calculated in comparison to a control. The three substances with the highest antiproliferative activity against the HT-29 cell line without HaCaT were identified based on the findings of the XTT investigation. XTT assays were repeated to determine three compounds at concentrations of 5 μg/ml, 10 μg/ml, 20 μg/ml, 50 μg/ml, and 100 μg/ml to calculate the $IC_{50}$ values. In addition, microscope images were taken to observe and evaluate the changes in the morphological features of the cells to which the three components with the highest cytotoxic activity on HT-29 cells were applied.

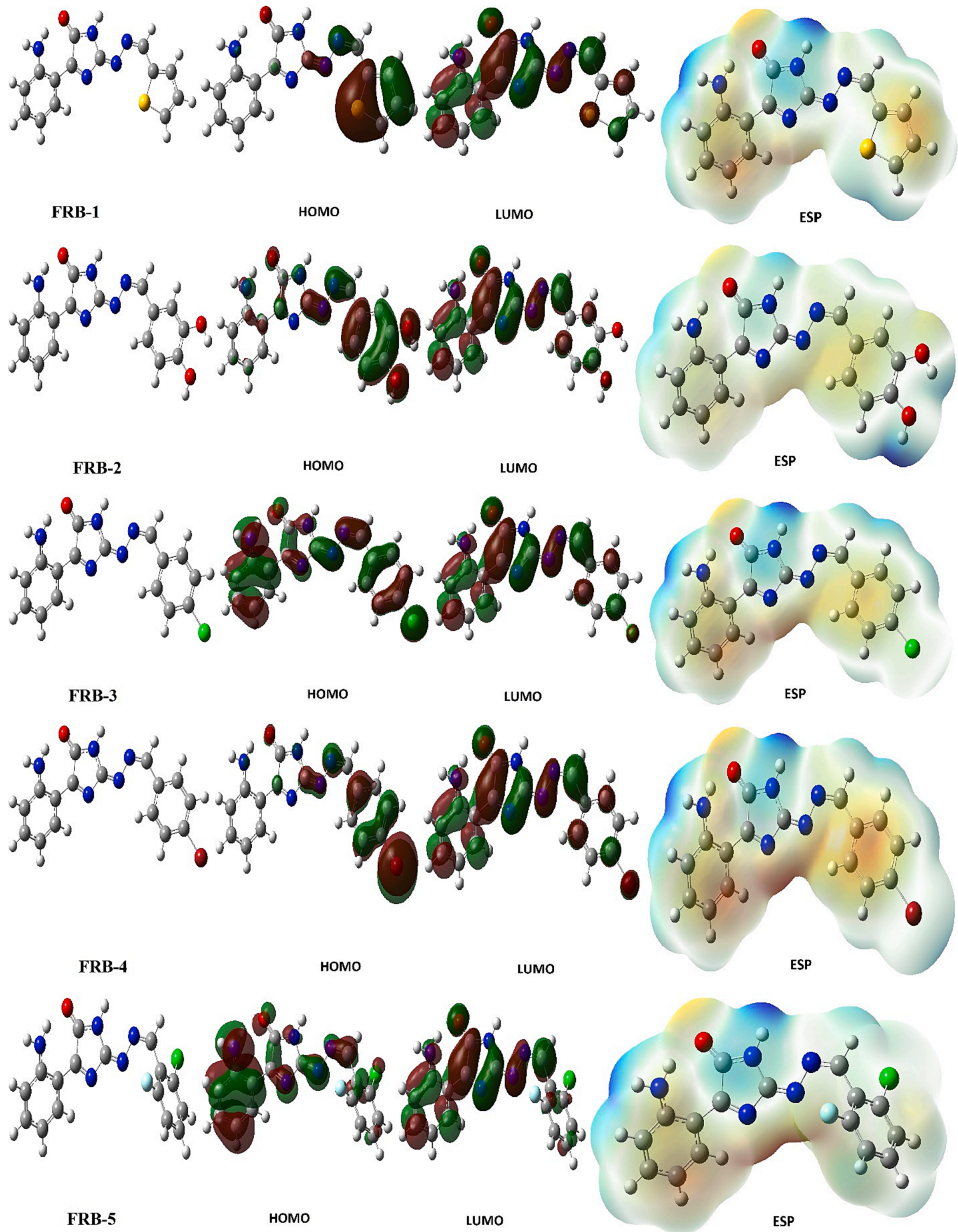


**Fig. 9.** Representations of optimized structure, HOMO, LUMO, and ESP of molecules.

### *2.4. Enzyme studies*

The enzyme activity of carbonic anhydrase was measured using the esterase activity technique. The technique is based on the esterase activity of CA. The method's basic idea is that the carbonic anhydrase enzyme's p-nitrophenylasetate is employed as a substrate. It undergoes hydrolysis to produce either p-nitrophenol or p-nitrophenol, which absorbs at 348 nm [39,40].

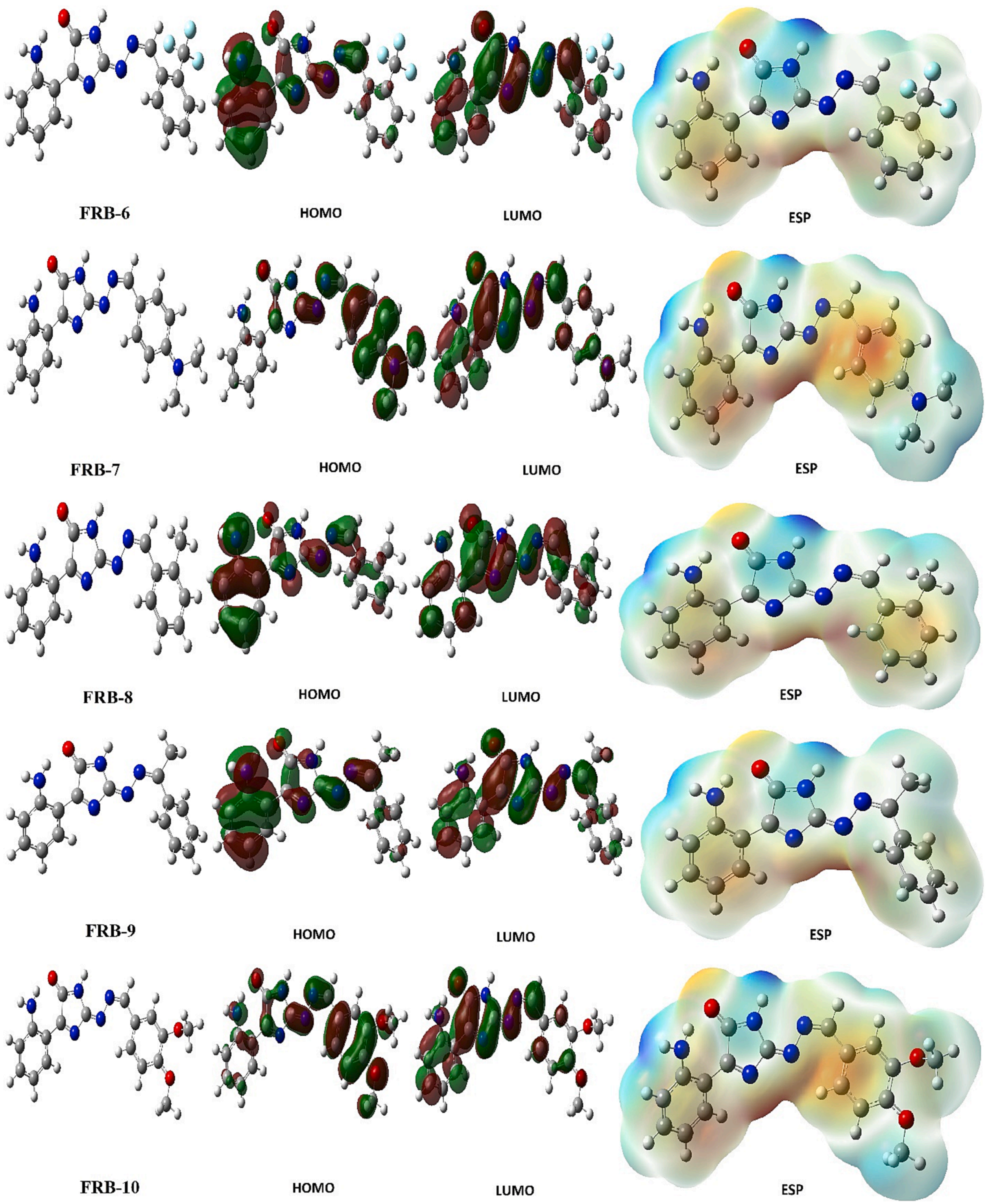


**Fig. 9.** (*continued*).

### 2.5. *Theoretical methods*

Theoretical calculations provide important information about the chemical and biological properties of molecules. Many quantum chemical parameters are obtained from theoretical calculations. The calculated parameters are used to explain the chemical activities of the molecules. Many programs are used to calculate molecules. These programs are Gaussian09 RevD.01 and GaussView 6.0. By using these programs, calculations were made in B3LYP, HF, and M06-2x methods with the 6-31++g(d,p) basis set. As a result of these calculations, many quantum chemical parameters have been found. Each parameter describes a different chemical property of molecules; the calculated parameters are calculated as follows:

$$\chi = -\left(\frac{\partial \mathrm{E}}{\partial \mathrm{N}}\right)_{\upsilon(r)} = \frac{1}{2}(I + A) \cong -\frac{1}{2}(E_{HOMO} + E_{LUMO})$$

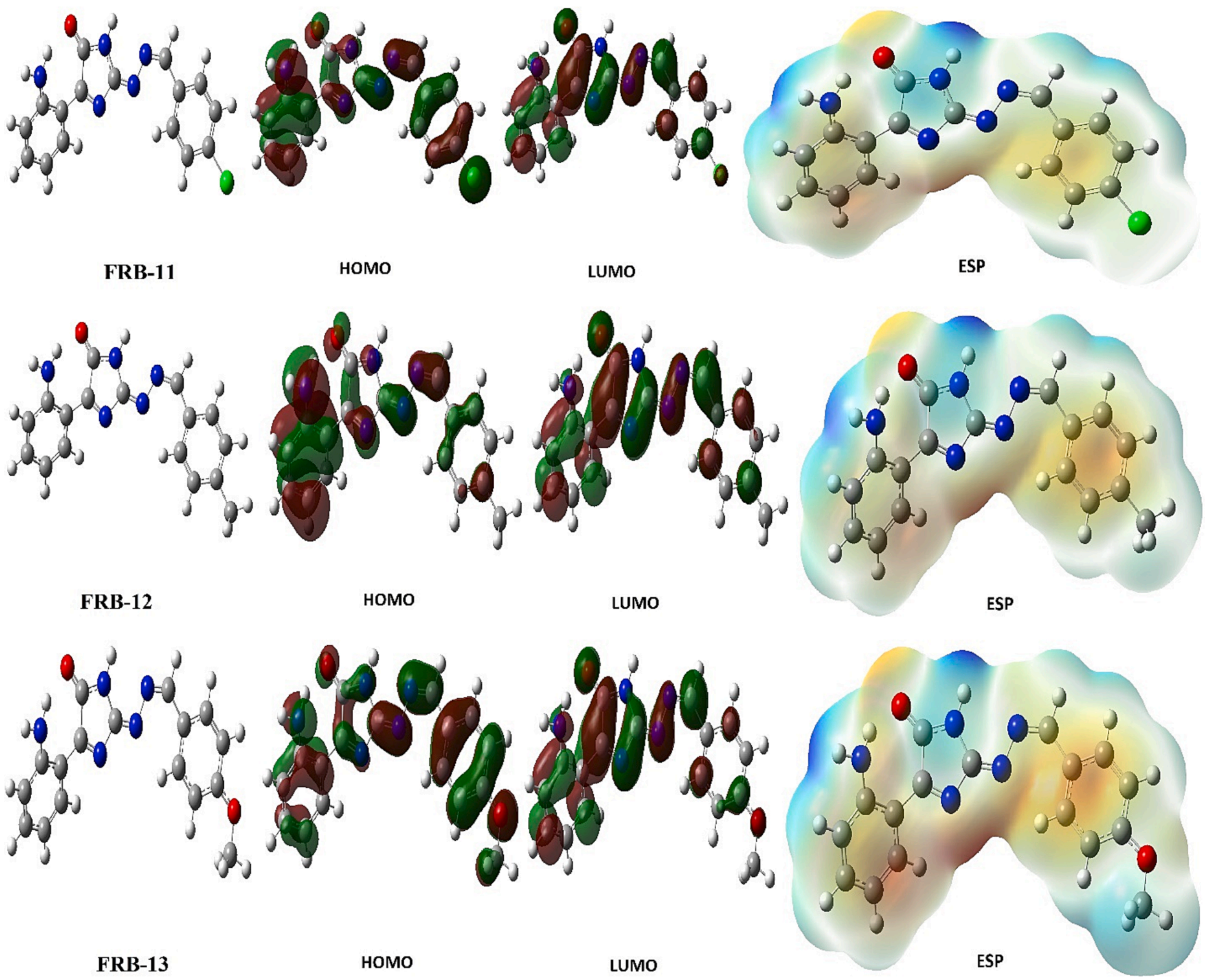


**Fig. 9.** (*continued*).

$$\eta = -\left(\frac{\partial^2 E}{\partial N^2}\right)_{\upsilon(r)} = \frac{1}{2}(I - A) \cong -\frac{1}{2}(E_{HOMO} - E_{LUMO})$$

$$\sigma = 1/\eta \quad \omega = \chi^2/2\eta \quad \varepsilon = 1/\omega$$

An important method used to determine the molecules with the highest activity against biological materials is molecular docking. Molecular docking calculations are made on Schrödinger's Maestro Molecular modeling platform (version 12.8). In the calculations made with this method, it is possible to comment on the active sites of the molecules. Calculations are made up of several steps. It first uses the protein preparation module to prepare the protein, then the LigPrep module to prepare the molecules. In order to interact with the prepared proteins and molecules, they interact with each other with the Glide ligand docking tool. Finally, the Qik-prop module of the Schrödinger software was used while performing ADME/T analysis (absorption, distribution, metabolism, excretion, and toxicity) in order to examine the effects of the studied molecules on human metabolism.

The binding free energy of ligand–protein complexes was found using the MM-GBSA method of the Prime module from Schrodinger. Other parameters were set by default. During the calculation, the OPLS3e force field, VSGB solvent model, and rotamer search algorithms were applied to define the bonding free energy. Here, we performed the binding free energy calculations of all complexes with the following equation:

$$\Delta G_{bind} = G_{complex} - (G_{protein} + G_{ligand})$$

where $\Delta G_{bind}$ is the binding free energy, $G_{complex}$ ligand–protein complexes are the free energy value, $G_{protein}$ is the target protein's free energy value, and $G_{ligand}$ is the free energy value of the ligand.

### 2.6. Statistical analysis

All experiments in this study were conducted three times, with the data being presented as the mean SEM. The one-way ANOVA Newman Tukey test was used to examine the acquired data, and differences were determined to be significant (p 0.05).

## 3. Results and discussions

### 3.1. Synthesis

The synthesis of target compounds **FRB (1–13)** is shown in Scheme 1. First, benzal aldehydes, or ketones, and aminogunidine hydrogen chloride were used to synthesize starting materials, 2-benzylidenehydrazinecarboximidamide derivatives, or guanylhydrzones (**III**). These compounds were synthesized in the presence of an inorganic base, potassium hydroxide, as described in the literature [41,42]. The target compounds were synthesized as a result of a condensation reaction between 2-benzylidenehydrazinecarboximidamide derivatives, or guanylhydrzones (**III**), and indole-2,3-dione in polar protic medium. In the

**Table 5**
Numerical values of the docking parameters of molecule against enzymes.

| 2CAB | Docking Score | Glide ligand efficiency | Glide hbond | Glide evdw | Glide ecoul | Glide emodel | Glide energy | Glide einternal | Glide posenum |
|---|---|---|---|---|---|---|---|---|---|
| FRB-1 | −5.50 | −0.26 | −0.42 | −36.00 | −4.63 | −52.80 | −40.63 | 2.27 | 340 |
| FRB-2 | −5.18 | −0.22 | −0.42 | −31.55 | −11.85 | −55.40 | −43.40 | 8.33 | 368 |
| FRB-3 | −4.03 | −0.18 | −0.44 | −32.36 | −7.64 | −52.80 | −39.99 | 4.79 | 396 |
| FRB-4 | −5.19 | −0.23 | −0.42 | −37.11 | −6.22 | −54.60 | −43.33 | 5.05 | 26 |
| FRB-5 | −4.92 | −0.20 | −0.42 | −36.97 | −5.35 | −55.51 | −42.33 | 3.05 | 293 |
| FRB-6 | −4.00 | −0.15 | −0.32 | −31.40 | −2.53 | −40.72 | −33.93 | 3.12 | 334 |
| FRB-7 | −5.31 | −0.21 | −0.06 | −32.10 | −2.01 | −44.55 | −34.11 | 2.74 | 312 |
| FRB-8 | −5.95 | −0.22 | −0.39 | −36.26 | −4.81 | −51.36 | −41.07 | 4.66 | 179 |
| FRB-9 | −4.87 | −0.21 | −0.16 | −37.43 | −3.23 | −52.37 | −40.65 | 1.64 | 390 |
| FRB-10 | −4.04 | −0.16 | 0.00 | −38.91 | −4.59 | −52.99 | −43.50 | 3.59 | 346 |
| FRB-11 | −4.03 | −0.18 | −0.44 | −32.40 | −7.62 | −52.82 | −40.02 | 4.79 | 396 |
| FRB-12 | −5.09 | −0.22 | −0.42 | −36.59 | −4.87 | −51.92 | −41.45 | 5.07 | 272 |
| FRB-13 | −5.05 | −0.21 | −0.44 | −35.56 | −5.79 | −52.81 | −41.35 | 3.27 | 307 |
| AZA | −4.29 | −0.12 | 0.00 | −44.38 | −4.97 | −62.08 | −49.35 | 3.70 | 352 |
| **3DC3** | **Docking Score** | **Glide ligand efficiency** | **Glide hbond** | **Glide evdw** | **Glide ecoul** | **Glide emodel** | **Glide energy** | **Glide einternal** | **Glide posenum** |
| FRB-1 | −4.70 | −0.22 | −0.32 | −33.38 | −5.92 | −49.12 | −39.30 | 2.65 | 141 |
| FRB-2 | −4.28 | −0.18 | 0.00 | −31.35 | −12.60 | −57.47 | −43.95 | 4.22 | 326 |
| FRB-3 | −4.54 | −0.20 | −0.32 | −34.26 | −7.47 | −51.73 | −41.73 | 5.73 | 332 |
| FRB-4 | −4.24 | −0.18 | −0.32 | −32.74 | −9.23 | −52.07 | −41.97 | 2.66 | 307 |
| FRB-5 | −4.29 | −0.18 | −0.32 | −31.98 | −6.18 | −47.75 | −38.16 | 2.30 | 159 |
| FRB-6 | −4.02 | −0.15 | −0.32 | −32.56 | −7.24 | −48.49 | −39.79 | 3.02 | 368 |
| FRB-7 | −4.06 | −0.16 | −0.32 | −33.24 | −6.32 | −47.87 | −39.56 | 3.72 | 131 |
| FRB-8 | −4.31 | −0.19 | −0.32 | −31.74 | −8.03 | −49.65 | −39.77 | 2.65 | 216 |
| FRB-9 | −5.47 | −0.24 | −0.32 | −33.42 | −7.05 | −53.05 | −40.48 | 2.51 | 178 |
| FRB-10 | −5.43 | −0.13 | −0.15 | −33.17 | −4.28 | −45.91 | −37.45 | 2.80 | 185 |
| FRB-11 | −4.54 | −0.20 | −0.32 | −34.22 | −7.51 | −51.74 | −41.73 | 5.73 | 332 |
| FRB-12 | −4.33 | −0.19 | −0.32 | −33.48 | −7.09 | −50.82 | −40.57 | 2.55 | 217 |
| FRB-13 | −5.05 | −0.21 | −0.50 | −35.61 | −8.58 | −55.88 | −44.18 | 5.56 | 102 |
| AZA | −4.64 | −0.13 | −0.47 | −43.67 | −9.56 | −66.84 | −53.23 | 10.27 | 110 |
| **4UYA** | **Docking Score** | **Glide ligand efficiency** | **Glide hbond** | **Glide evdw** | **Glide ecoul** | **Glide emodel** | **Glide energy** | **Glide einternal** | **Glide posenum** |
| FRB-1 | −5.32 | −0.25 | 0.00 | −33.11 | −9.69 | −57.76 | −42.80 | 1.81 | 50 |
| FRB-2 | −7.17 | −0.30 | 0.00 | −29.80 | −44.30 | −109.16 | −74.10 | 6.30 | 288 |
| FRB-3 | −6.52 | −0.28 | −0.12 | −32.06 | −40.46 | −109.39 | −72.52 | 3.05 | 120 |
| FRB-4 | −6.09 | −0.26 | −0.13 | −30.14 | −40.21 | −103.89 | −70.34 | 3.25 | 354 |
| FRB-5 | −6.03 | −0.25 | −0.13 | −27.56 | −39.83 | −101.45 | −67.40 | 0.84 | 253 |
| FRB-6 | −5.71 | −0.22 | −0.13 | −28.86 | −38.95 | −95.11 | −67.82 | 2.03 | 110 |
| FRB-7 | −6.57 | −0.26 | −0.12 | −34.32 | −41.15 | −114.24 | −75.48 | 1.93 | 363 |
| FRB-8 | −7.18 | −0.27 | −0.13 | −29.65 | −41.17 | −107.26 | −70.82 | 0.81 | 229 |
| FRB-9 | −6.66 | −0.29 | −0.13 | −33.53 | −42.91 | −115.89 | −76.44 | 2.07 | 293 |
| FRB-10 | −6.44 | −0.25 | −0.16 | −37.74 | −13.13 | −72.02 | −50.87 | 4.51 | 178 |
| FRB-11 | −6.52 | −0.28 | −0.12 | −32.06 | −40.46 | −109.39 | −72.52 | 3.05 | 120 |
| FRB-12 | −6.37 | −0.28 | −0.10 | −31.93 | −38.42 | −105.84 | −70.35 | 4.35 | 173 |
| FRB-13 | −6.63 | −0.28 | −0.09 | −33.82 | −38.71 | −108.71 | −72.53 | 7.75 | 360 |
| **3DTC** | **Docking Score** | **Glide ligand efficiency** | **Glide hbond** | **Glide evdw** | **Glide ecoul** | **Glide emodel** | **Glide energy** | **Glide einternal** | **Glide posenum** |
| FRB-1 | −3.83 | −0.18 | −0.17 | −29.95 | −4.29 | −39.54 | −34.24 | 1.80 | 327 |
| FRB-2 | −3.63 | −0.15 | −0.34 | −25.80 | −7.29 | −40.55 | −33.09 | 2.64 | 398 |
| FRB-3 | −3.42 | −0.15 | −0.56 | −21.12 | −8.24 | −35.78 | −29.36 | 5.65 | 288 |
| FRB-4 | −3.22 | −0.14 | −0.32 | −27.65 | −4.02 | −36.75 | −31.67 | 3.75 | 148 |
| FRB-5 | −3.73 | −0.16 | 0.00 | −33.64 | −4.09 | −45.49 | −37.73 | 2.03 | 286 |
| FRB-6 | −3.21 | −0.12 | −0.31 | −28.58 | −2.11 | −37.02 | −30.70 | 0.51 | 286 |
| FRB-7 | −2.60 | −0.10 | 0.00 | −31.48 | −0.05 | −36.23 | −31.52 | 1.79 | 357 |
| FRB-8 | −3.46 | −0.15 | −0.30 | −27.84 | −2.48 | −37.04 | −30.32 | 0.59 | 385 |
| FRB-9 | −3.10 | −0.13 | −0.32 | −28.02 | −2.24 | −36.12 | −30.26 | 0.46 | 11 |
| FRB-10 | −3.07 | −0.12 | −0.32 | −27.07 | −1.34 | −34.16 | −28.41 | 0.89 | 387 |

(continued on next page)

**Table 5** (*continued*)

| 2CAB | Docking Score | Glide ligand efficiency | Glide hbond | Glide evdw | Glide ecoul | Glide emodel | Glide energy | Glide einternal | Glide posenum |
|---|---|---|---|---|---|---|---|---|---|
| FRB-11 | −3.42 | −0.15 | −0.56 | −21.12 | −8.24 | −35.78 | −29.36 | 5.65 | 288 |
| FRB-12 | −2.99 | −0.13 | −0.32 | −27.37 | −1.47 | −34.38 | −28.84 | 0.28 | 244 |
| FRB-13 | −3.19 | −0.13 | −0.59 | −22.39 | −8.62 | −36.67 | −31.01 | 6.66 | 176 |

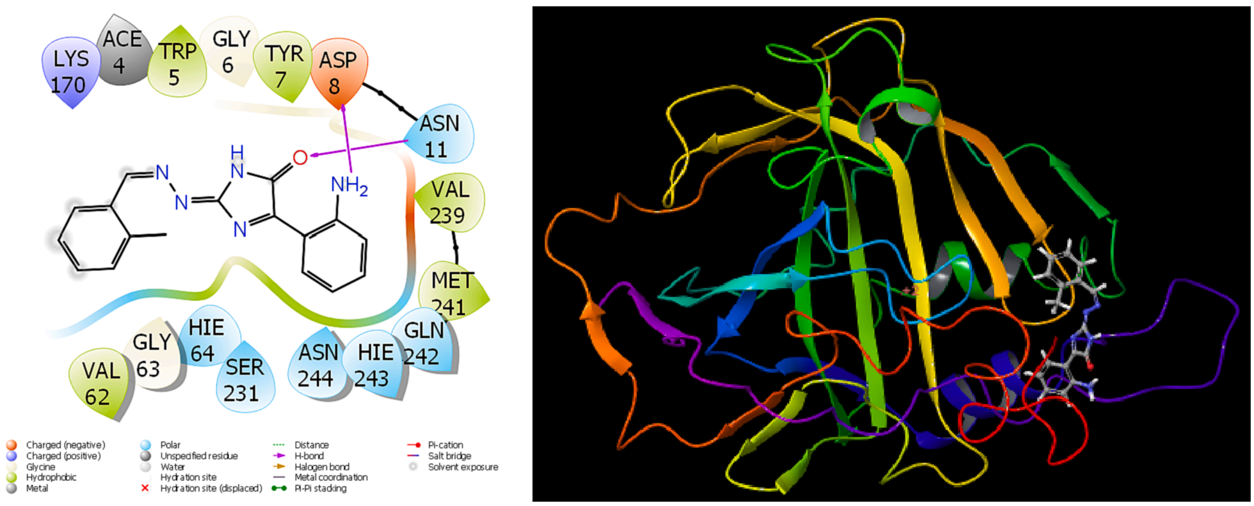


**Fig. 10.** Docking interactions of **FRB-8** and hCA I enzyme protein.

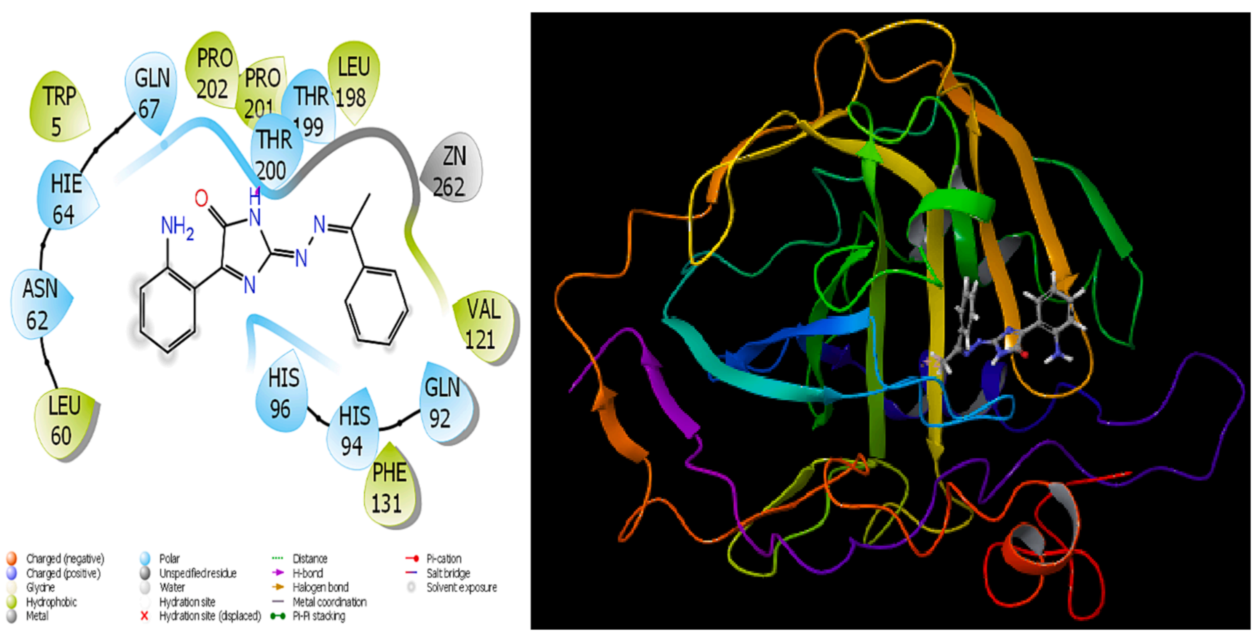


**Fig. 11.** Docking interactions of **FRB-10** with hCA II enzyme protein.

literature, the reaction of aminoguanidine hydrochloride and isatin was reported to furnish 2-(2-oxoindolin-3-ylidene)hydrazine-1-carboximidamide [58], but in this work, we report a guanylhydrazone (**III**) reaction with isatin to give 5-imidazol-4-one derivatives, **FRB (1–13)**. The synthesized compounds were subjected to purification through recrystallization, utilizing ethyl acetate as the solvent. Table 1 depicts the structural characteristics and physical properties of the synthesized compounds FRB(1–13). The probable mechanism for the formation of target compounds is illustrated in Scheme 2. The structure of synthesized compounds was confirmed by using several spectral techniques, including $^{1}$H NMR, $^{13}$C NMR, FTIR, and HRMS. The analytical data for the synthesized compounds were presented in the experimental section.

The distinctive absorption bands were observed in the IR spectra at 3320–3240 $cm^{-1}$ corresponding to NH, 1850–1541 $cm^{-1}$ for the imine stretching frequency, and 1670–1540 $cm^{-1}$ due to the frequency of carbonyl stretching. Target compounds' proton NMR spectra display representative chemical shift values at 8.10–8.34 ppm, which

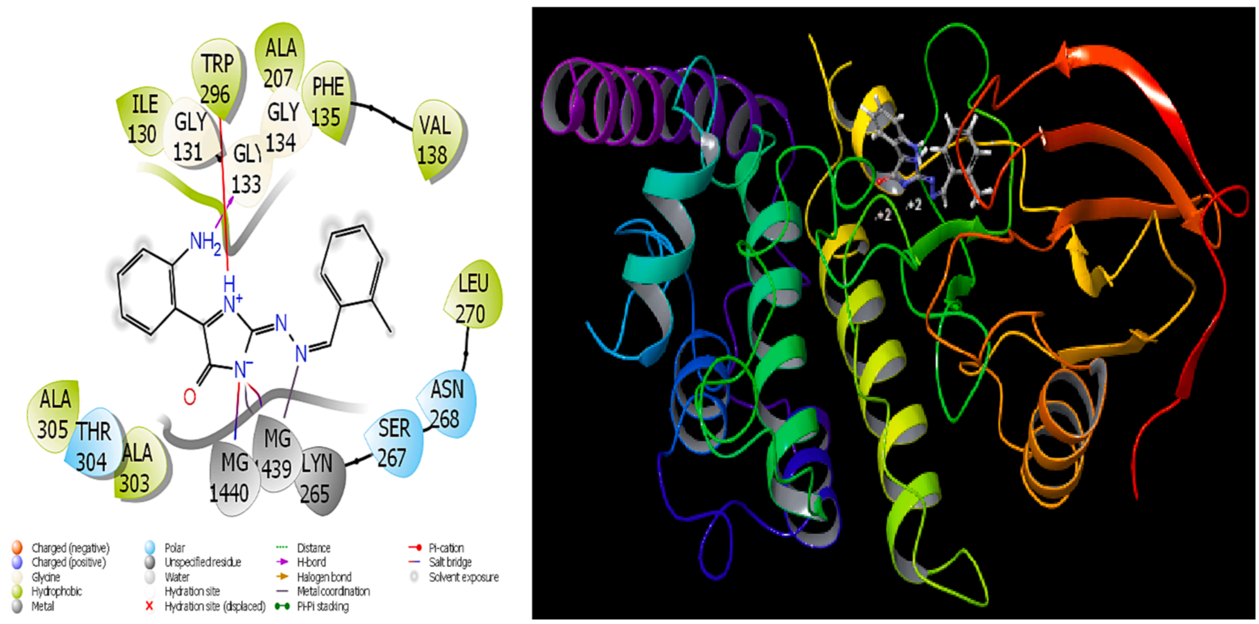


**Fig. 12.** Docking interactions of FRB-8 with colon cancer protein (4UYA).

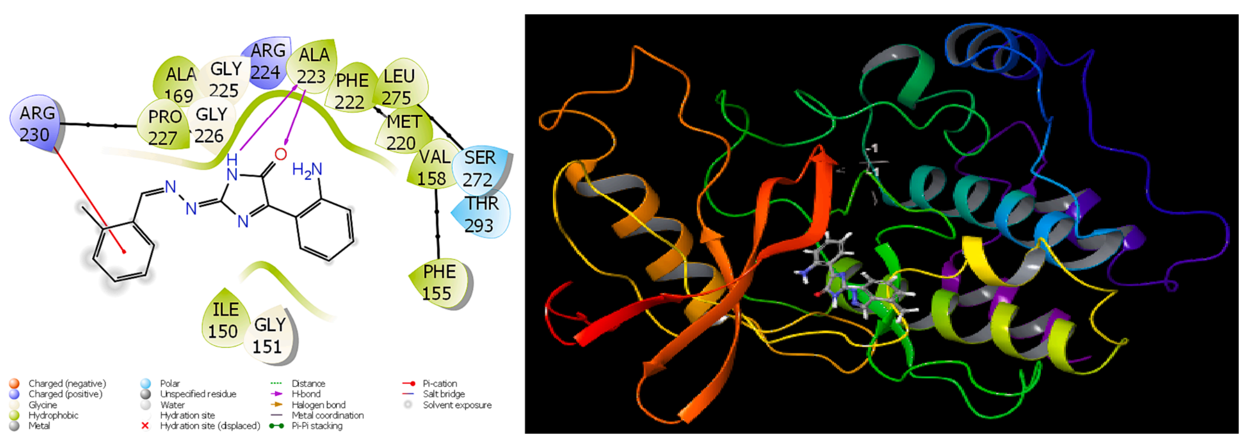


**Fig. 13.** Docking interactions of FRB-8 with colon cancer protein (3DTC).

**Table 6**
MM-GBSA parameter of molecule (kcal/mol).

| | FRB 1 | FRB 2 | FRB 3 | FRB 4 | FRB 5 | FRB 6 | FRB 7 | FRB 8 | FRB 9 | FRB 10 | FRB 11 | FRB 12 | FRB 13 |
|---|---|---|---|---|---|---|---|---|---|---|---|---|---|
| $\Delta G_{Binding\ energy}$ | −10.64 | −9.37 | −9.72 | −6.36 | −6.74 | −6.73 | 8.13 | −7.77 | −2.53 | −10.74 | −1.48 | 2.44 | 20.71 |
| $\Delta G_{Binding\ Coulomb}$ | −30.06 | −26.03 | −21.61 | −25.34 | −23.11 | −23.10 | −23.42 | −21.78 | −19.94 | −22.91 | −14.92 | −18.91 | −31.66 |
| $\Delta G_{Binding\ Covalent}$ | 1.99 | 6.39 | 1.15 | 3.52 | 5.46 | 5.45 | 11.46 | 1.06 | 3.19 | 5.65 | 3.68 | 5.35 | 2.99 |
| $\Delta G_{Binding\ Hbond}$ | −0.54 | −0.58 | −0.11 | −0.59 | −0.59 | −0.59 | −0.87 | −0.12 | −0.40 | −0.59 | −0.40 | −0.56 | −0.67 |
| $\Delta G_{Binding\ Lipo}$ | −12.60 | −14.46 | −17.36 | −14.01 | −13.59 | −13.59 | −20.02 | −15.33 | −11.25 | −12.68 | −11.81 | −10.25 | −14.76 |
| $\Delta G_{Binding\ Packing}$ | −0.29 | −0.08 | −1.07 | −0.20 | −0.10 | −0.10 | −0.21 | −0.85 | −0.02 | −0.09 | −0.02 | −0.06 | −0.96 |
| $\Delta G_{Binding\ Solv\ GB}$ | 66.54 | 66.25 | 66.40 | 69.77 | 63.55 | 63.56 | 82.91 | 64.92 | 58.66 | 64.05 | 56.90 | 64.41 | 103.09 |
| $\Delta G_{Binding\ vdW}$ | −35.68 | −40.85 | −37.11 | −39.51 | −38.35 | −38.35 | −41.71 | −35.67 | −32.77 | −39.17 | −34.91 | −37.53 | −37.32 |

correspond to methylenimine proton [43], 12.90–12.20 ppm corresponding to imidazole NH, and 7.79–7.89 ppm due to the amino phenyl group (Ar-$NH_2$) [44]. The carbon NMR showed representative peaks for the carbonyl, carbon two of the imidazole, and imine at 164–168, 163–159, and 142–137 ppm, respectively. The molecular ion peak *m/z* of all the synthesized compounds obtained from HRMS were observed to be consistent with the calculated values. Furthermore, the compound FRB-1 exhibited a highly fragmented ion in addition to the molecular ion at 213.1453 amu, which was identified as $C_{10}H_8N_5O^+$.

## 3.2. Cytotoxicity studies

The synthesized 5-imidazol-4-one derivatives were evaluated for their in vitro anticancer activity towards both a normal (HaCaT cell line) and cancer cell line, the Human Colorectal Adenocarcinoma Cell Line (HT-29 cell line). These compounds exhibited interesting anticancer activity on a cancerous cell line and less cytotoxic effects on a healthy cell line, as shown in Fig. 3 by the XTT cytotoxicity studies. Compounds were evaluated at a single concentration of 20 μg/ml. The cell viability

**Table 7**
ADME properties of molecule.

| | FRB 1 | FRB 2 | FRB 3 | FRB 4 | FRB 5 | FRB 6 | FRB 7 | Referance Range |
|---|---|---|---|---|---|---|---|---|
| mol_MW | 297 | 323 | 326 | 370 | 344 | 359 | 334 | 130–725 |
| dipole (D) | 3.3 | 5.1 | 2.9 | 2.7 | 3.2 | 2.3 | 3.8 | 1.0–12.5 |
| SASA | 574 | 621 | 620 | 625 | 618 | 619 | 665 | 300–1000 |
| FOSA | 24 | 28 | 28 | 28 | 25 | 20 | 169 | 0–750 |
| FISA | 180 | 283 | 180 | 180 | 173 | 171 | 190 | 7–330 |
| PISA | 336 | 311 | 341 | 340 | 325 | 338 | 306 | 0–450 |
| WPSA | 35 | 0 | 72 | 77 | 94 | 90 | 0 | 0–175 |
| volume ($A^3$) | 958 | 1043 | 1041 | 1049 | 1044 | 1066 | 1135 | 500–2000 |
| donorHB | 2.5 | 4.5 | 2.5 | 2.5 | 2.5 | 2.5 | 2.5 | 0–6 |
| accptHB | 7.5 | 9 | 7.5 | 7.5 | 7.5 | 7.5 | 8.5 | 2.0–20.0 |
| glob (Sphere = 1) | 0.8 | 0.8 | 0.8 | 0.8 | 0.8 | 0.8 | 0.8 | 0.75–0.95 |
| QPpolrz ($A^3$) | 32.8 | 34.7 | 36.2 | 36.5 | 36.2 | 37.2 | 39.0 | 13.0–70.0 |
| QPlogPC16 | 11.4 | 13.0 | 12.6 | 12.7 | 12.1 | 11.7 | 12.8 | 4.0–18.0 |
| QPlogPoct | 19.0 | 23.8 | 20.3 | 20.4 | 20.4 | 20.7 | 21.4 | 8.0–35.0 |
| QPlogPw | 14.8 | 19.4 | 14.9 | 15.0 | 14.8 | 14.9 | 15.6 | 4.0–45.0 |
| QPlogPo/w | 1.3 | 0.1 | 1.9 | 2.0 | 2.1 | 2.2 | 1.7 | −2.0–6.5 |
| QPlogS | −3.7 | −3.6 | −4.6 | −4.7 | −4.7 | −4.6 | −4.6 | −6.5–0.5 |
| CIQPlogS | −3.3 | −3.3 | −3.9 | −4.7 | −4.2 | −4.5 | −3.7 | −6.5–0.5 |
| QPlogHERG | −6.1 | −6.2 | −6.4 | −6.4 | −6.2 | −6.1 | −6.4 | * |
| QPPCaco (nm/sec) | 195 | 21 | 196 | 196 | 225 | 238 | 157 | ** |
| QPlogBB | −1.4 | −2.7 | −1.4 | −1.4 | −1.2 | −1.2 | −1.8 | −3.0–1.2 |
| QPPMDCK (nm/sec) | 131 | 7 | 212 | 226 | 324 | 326 | 67 | ** |
| QPlogKp | −3.3 | −5.1 | −3.2 | −3.2 | −3.2 | −3.1 | −3.5 | Kp in cm/hr |
| IP (ev) | 8.3 | 8.4 | 8.4 | 8.5 | 8.4 | 8.5 | 8.3 | 7.9–10.5 |
| EA (eV) | 1.6 | 1.2 | 1.3 | 1.3 | 1.3 | 1.3 | 1.1 | −0.9–1.7 |
| #metab | 4 | 5 | 3 | 3 | 3 | 4 | 4 | 1–8 |
| QPlogKhsa | −0.3 | −0.5 | −0.2 | −0.2 | −0.2 | −0.1 | −0.2 | −1.5–1.5 |
| Human Oral Absorption | 3 | 2 | 3 | 3 | 3 | 3 | 3 | – |
| Percent Human Oral Absorption | 76 | 51 | 79 | 80 | 81 | 83 | 76 | *** |
| PSA | 112 | 158 | 113 | 113 | 112 | 112 | 119 | 7–200 |
| RuleOfFive | 0 | 0 | 0 | 0 | 0 | 0 | 0 | Maximum is 4 |
| RuleOfThree | 0 | 1 | 0 | 0 | 0 | 0 | 0 | Maximum is 3 |
| Jm | 0.0 | 0.0 | 0.0 | 0.0 | 0.0 | 0.0 | 0.0 | – |

| | FRB 8 | FRB 9 | FRB 10 | FRB 11 | FRB 12 | FRB 13 | Referance Range |
|---|---|---|---|---|---|---|---|
| mol_MW | 305 | 305 | 351 | 326 | 305 | 321 | **130–725** |
| dipole (D) | 3.0 | 3.8 | 4.0 | 2.9 | 3.0 | 4.0 | **1.0–12.5** |
| SASA | 617 | 624 | 652 | 620 | 627 | 625 | **300–1000** |
| FOSA | 92 | 83 | 189 | 28 | 115 | 116 | **0–750** |
| FISA | 174 | 172 | 180 | 180 | 180 | 180 | **7–330** |
| PISA | 350 | 369 | 284 | 340 | 332 | 329 | **0–450** |
| WPSA | 0 | 0 | 0 | 72 | 0 | 0 | **0–175** |
| volume (A3) | 1042 | 1051 | 1128 | 1039 | 1053 | 1064 | **500–2000** |
| donorHB | 2.5 | 2.5 | 2.5 | 2.5 | 2.5 | 2.5 | **0–6** |
| accptHB | 7.5 | 7 | 9 | 7.5 | 7.5 | 8.25 | **2.0–20.0** |
| glob (Sphere = 1) | 0.8 | 0.8 | 0.8 | 0.8 | 0.8 | 0.8 | **0.75–0.95** |
| QPpolrz (A3) | 36.3 | 36.9 | 37.8 | 36.1 | 36.6 | 36.4 | **13.0–70.0** |
| QPlogPC16 | 12.1 | 12.3 | 12.5 | 12.5 | 12.1 | 12.2 | **4.0–18.0** |
| QPlogPoct | 20.0 | 20.0 | 21.3 | 20.3 | 20.1 | 20.5 | **8.0–35.0** |
| QPlogPw | 14.9 | 14.6 | 15.6 | 14.9 | 14.9 | 15.4 | **4.0–45.0** |
| QPlogPo/w | 1.7 | 2.0 | 1.6 | 1.9 | 1.7 | 1.5 | **−2.0–6.5** |
| QPlogS | −4.2 | −4.4 | −4.1 | −4.6 | −4.3 | −4.0 | **−6.5–0.5** |
| CIQPlogS | −3.5 | −3.7 | −3.9 | −3.9 | −3.5 | −3.6 | **−6.5–0.5** |
| QPlogHERG | −6.3 | −6.5 | −6.1 | −6.4 | −6.4 | −6.2 | * |
| QPPCaco (nm/sec) | 223 | 232 | 196 | 196 | 196 | 196 | ** |
| QPlogBB | −1.5 | −1.5 | −1.7 | −1.4 | −1.6 | −1.6 | **−3.0–1.2** |
| QPPMDCK (nm/sec) | 98 | 102 | 85 | 211 | 85 | 85 | ** |
| QPlogKp | −3.1 | −3.0 | −3.3 | −3.3 | −3.3 | −3.2 | **Kp in cm/hr** |
| IP (ev) | 8.3 | 8.2 | 8.4 | 8.4 | 8.3 | 8.4 | **7.9–10.5** |
| EA (eV) | 1.1 | 1.1 | 1.2 | 1.3 | 1.1 | 1.2 | **−0.9–1.7** |
| #metab | 4 | 4 | 5 | 3 | 4 | 4 | **1–8** |
| QPlogKhsa | −0.2 | −0.1 | −0.3 | −0.2 | −0.1 | −0.3 | **−1.5–1.5** |
| Human Oral Absorption | 3 | 3 | 3 | 3 | 3 | 3 | **–** |
| Percent Human Oral Absorption | 79 | 81 | 77 | 79 | 78 | 77 | *** |
| PSA | 112 | 112 | 128 | 113 | 113 | 122 | **7–200** |
| RuleOfFive | 0 | 0 | 0 | 0 | 0 | 0 | **Maximum is 4** |
| RuleOfThree | 0 | 0 | 0 | 0 | 0 | 0 | **Maximum is 3** |
| Jm | 0.0 | 0.0 | 0.0 | 0.0 | 0.0 | 0.0 | **–** |

* corcern below −5, **<25 is poor and > 500 is great, *** <25 % is poor and > 80 % is high.

rates of these compounds on the HT-29 cell line ranged from 50.62 ± 0.19 % to 83.47 ± 0.34 %. Compounds **FRB-1**, **FRB-4,** and **FRB-8** exhibited significant antiproliferative activity with cell viability rates of 50.620.19 %, 55.230.31 %, and 58.320.32 %, respectively. The synthesized compound **FRB 11** displayed the lowest cytotoxic activity, with a cell viability rate of 83.47 ± 0.34 %. On the application of imatinib to HT-29 cells at the same concentration, cell viability was calculated as 62.98 ± 0.32 %. According to the results of the study on the HT-29 cell line, **FRB-1**, **FRB-4**, and **FRB-8** compounds had more effective cytotoxic activity than imatinib.

A XTT cell viability assay was also executed on the HaCaT cell line, and it was noticed that the compounds treated at the same concentration did not display a cytotoxic effect on the cells. Therefore, the cell viability was above 70 %, which was important and critical. According to cell viability study results, HaCaT cell viability rates were between 74.52 ± 0.29 % **FRB-10** and 90.39 ± 0.38 % **FRB-8**. In light of the findings, it can be concluded that these compounds had trivial toxic properties on the HaCaT cell line, as depicted in Fig. 4. In addition, it was also deduced that a well-known commercially available anticancer agent, "Imatinib," that was used as a reference compound in this assay had more toxic effect properties on a healthy cell line as compared to the synthesized compounds, proving the biocompatibility of synthesized compounds with Imatinib. To calculate the $IC_{50}$ values of the most active compounds among the synthesized 5-imidazol-4-one derivatives, **FRB-1**, **FRB-4,** and **FRB-8** in the HT-29 cell line were treated to the cells at 5 different concentrations, and the XTT assay was carried out to kill 50 % of the cells (see Fig. 5).

When the XTT test was done on HT-29 cells, the rates of cell survival were inversely related to the concentrations of the synthesized compounds that were used. HT-29 cell viability rates were calculated as **FRB-1** (65.09 ± 0.48 %), **FRB-4** (71.15 ± 0.35 %), **FRB-8** (60.51 ± 0.32 %), and imatinib (73.25 ± 0.23 %) when the specified compounds were administered at a concentration of 5 μg/ml. Thenceforth, at a concentration of 100 μg/ml, the synthesized compounds were treated with the HT-29 cells, and the cell viability was calculated as **FRB-1** (36.32 ± 0.49 %), **FRB-4** (40.75 ± 0.42 %), **FRB-8** (34.09 ± 0.26 %), and imatinib (46.24 ± 0.47 %). As shown in Fig. 6, the IC50 values for imatinib, **FRB-1**, **FRB-4**, and **FRB-8** compounds were determined to be 36.78 ± 0.17 μg/ml, 49.76 ± 0.22 μg/ml, 30.84 ± 0.19 μg/ml, and 57.34 ± 0.25 μg/ml, respectively (Table 2). The $IC_{50}$ values of the three compounds, **FRB-1**, **FRB-4**, and **FRB-8,** were lower than those of imatinib. Based on these findings, it can be stated that these synthesized compounds have more antiproliferative activity against the HT-29 cell line and are more effective candidates than imatinib, which was used as a reference.

The HaCaT cell line was also subjected to imatinib and five distinct concentrations of synthesized compounds, and the results were assessed. According to the results in Fig. 6, it was observed that these compounds and imatinib did not kill 50 % or more of the cells at the treated concentrations. In this case, the $IC_{50}$ value could not be calculated. The compounds were treated with the HaCaT cells at a concentration of 100 μg/ml, and the cell viability was calculated as **FRB-1** (68.77 ± 0.8 %), **FRB-4** (66.73 ± 0.37 %), **FRB-8** (62.66 ± 0.51 %) and imatinib (55.24 ± 0.31 %).

The morphological properties of the synthesized 5-imidazol-4-one derivatives (**FRB-1**, **FRB-4**, and **FRB-8**) with the greatest cytotoxic activities in the HT-29 colon cancer cell line were evaluated by taking microscope images. Morphological features of cells were performed 24 h after 20 μg/mL of compounds **FRB-1**, **FRB-4,** and **FRB-8** were applied to HT-29 and HaCaT cell lines in Fig. 6. Significant morphological changes in the cells were observed between cells that were treated with the title compounds (**FRB-1**, **FRB-4**, and **FRB-8**) and the HT-29 control group. According to Fig. 7, which shows microscopic image results of HaCaT cells treated with 5-imidazol-4-one derivatives (**FRB-1**, **FRB-4**, and **FRB-8**) derivatives, it can be inferred that these compounds caused a lower rate of morphological difference compared to HT-29 cells.

### *3.3. Carbonic anhydrases inhibition activity*

The inhibition potentials of the synthesized 5-imidazol-4-one derivatives **FRB (1–13)** against two physiologically relevant CA isoforms, which are the slower cytosolic isoform (hCA I) and the more rapid cytosolic isoenzyme (hCA II), were investigated by using an esterase assay method. The inhibition data of the title compounds **FRB (1–13)** against CA I and CA II isoforms were summarized in Table 3 and Fig. 8 ($IC_{50}$ and $K_i$ values expressed as nanomolar (nM)).

The title compounds, **FRB (1–13),** significantly inhibited both the cytosolic isoforms hCA I and hCA II, with $IC_{50}$ ranging between 0.5940 and 1.8570 nM for hCA I and $IC_{50}$ ranging between 0.1904 and 1.8280 nM for hCA II. **FRB-1 and FRB-7** were found to be excellent inhibitors for these isoforms, hCA I and hCA II, with $IC_{50}$ values of 0.1904 and 0.5940 nM, respectively. The Ki values were found to be in the range of 6.49 ± 1.010–739.12 ± 111.35 nM for hCA I (Ki value for standard inhibitor = 271.15 ± 74.620 nM) and 64.53 ± 19.44–314.37 ± 54.78 nM for hCA II (Ki value for standard inhibitor = 113.07 ± 20.980 nM).

### *3.4. Computational studies: DFT studies, molecular docking and ADME/T*

#### *3.4.1. DFT studies*

With theoretical calculations, it is possible to have a lot of information about the molecule. Among these theoretical calculations, one of the most widely used is the Gaussian software program, which gives important information about many chemical properties of molecules. To compare the activities of molecules, the numerical values of two parameters of molecules are used, which are HOMO and LUMO. The HOMO parameter of molecules shows the ability of molecules to donate electrons, and it is known that the activity of the molecule with the most positive numerical value of this parameter is the highest [46]. On the other hand, the LUMO parameter of the molecules shows the electron-accepting capacity of the molecule, which shows that the activity of the molecule with the most negative numerical value of this parameter is higher than that of other molecules [47]. The numerical value of these two parameters allows for interpretation of the activity of molecules. Apart from these two parameters, it is predicted that the activity of the molecule with the smallest numerical value of the $\Delta E$ parameter is higher than that of other molecules.

Another calculated parameter is electronegativity. The electronegativity parameter shows the strength of the atoms in the molecule to attract bond electrons. As the numerical value of this parameter increases, its electronegative value will increase, which will decrease the activity of the molecule. Many more parameters are calculated, and it should be noted that each parameter gives information about the different properties of the molecules, among which these four parameters are more important than the others [48]. All parameters are given in Table 4.

Although many parameters have been obtained as a result of the calculations, very few are visualized. The visuals for these parameters are given in Fig. 9. There are four different pictures in these images, the first of which is the picture of the optimized structure of molecules. The next two pictures show on which atoms the HOMO and LUMO orbitals of the molecules are concentrated. In the last picture, the electrostatic potential (ESP) of the molecules is given. In these pictures, there is a color scale from blue to red, which shows the regions with the lowest electron density. The red color indicates the regions with the highest electron density [49].

#### *3.4.2. Molecular docking*

It is possible to make molecular docking calculations in order to compare the activities of the studied molecules (5-imidazol-4-one derivatives, **FRB (1–13)** against biological materials. With these calculations, it is possible to predict the active sites of molecules and examine the interactions of molecules with proteins, which are biological materials. During molecular docking calculations, the most important factor determining the activities of molecules is the interactions between molecules and proteins, and as a result of these interactions, molecules try to inhibit proteins [50]. For this reason, the chemical interactions between the molecule and the protein have gained great importance, which are hydrogen bonds, polar and hydrophobic interactions, π-π, and halogen [51]. In light of the above information, it is seen that as these chemical interactions increase, the activities of the molecules increase.

As a result of the calculations, the activities of the molecules against various proteins are compared. For this comparison, the docking score parameter is made according to its numerical value, and the most negative numerical value of this parameter has the highest activity. Although many parameters except the docking score parameter are calculated in the molecular docking calculations, the parameters that have an effect on the activity are quite limited, and parameters such as Glide ligand efficiency, Glide hbond, Glide evdw, and Glide ecoul give numerical values obtained for the interaction between molecules and proteins [52]. On the other hand, the four calculated parameters, Glide emodel, Glide energy, Glide einternal, and Glide posenum, give the numerical values obtained for the pose formed as a result of the interaction [53]. All parameters are given in Table 5.

As a result of the calculations, when the interaction of the molecule **FRB-8** with the hCA I protein was examined in detail, as shown in Fig. 10, a hydrogen bond interaction occurred between the phenyl amino group of the **FRB-8** molecule and the ASP 8 protein. In addition, a hydrogen bond interaction with the ASN-11 protein occurred with the oxygen atom in the imidazole ring in the same molecule. In Fig. 11, it is seen that the molecule **FRB-10** generally produces hydrophilic interactions, polar interactions, and unspecified residue interactions with proteins found in the hCA II protein. On the other hand, in Fig. 12, when the molecule **FRB-8** interacts with the colon cancer (4UYA) protein, a hydrogen bond interaction is created with the GLY 133 protein in the amino phenyl group in the molecule. The nitrogen atom in the imidazole ring in the same molecule creates a Pi-cation interaction with the TRP 296 protein. It is seen that the other nitrogen atoms in the same ring, Mg 1439 and Mg 1440, create a salt bridge interaction. Besides, it is seen that metal coordination interaction occurs with the nitrogen atom Mg 1439 metal in the middle of the methylenehydrazine group. Finally, in the interaction of the molecule FRB-8 with the colon cancer (3DTC) protein in Fig. 13, the oxygen atom as part of the carbonyl adjacent to the imidazole ring creates a hydrogen bond interaction with the ALA 223 protein, and the nitrogen atom in the imidazole group interacts with the ALA 223 protein. However, the phenyl ring at the other end of the molecule appears to interact with the ARG 230 protein.

As a result of the MM-GBSA calculations, the binding free energy values of each molecule were found separately. As a result of the calculations, the energy values of the molecule against colon cancer proteins are given in Table 6. In these calculations, MM-GBSA values are obtained from the interaction of the molecule with the 4UYA proteins. The numerical value of the $\Delta G_{\text{Binding energy}}$ parameter in the MM-GBSA calculations of the molecules is −10.74 for the FRB-10 molecule, while the most positive value is **FRB-13** with 20.71. It has been mentioned in molecular docking calculations that there are many interactions between molecules and proteins. These interactions are Coulomb, covalent, Hbond, lipophilic, packaging, SolvGB, and vdW interactions [54]. Each interaction has been found to be of greater importance for different molecules. For example, Lipo (lipophilic) and vdw (van der Waals) interactions are more common in the molecule's interactions with proteins.

### 3.4.3. *ADME/T analysis*

After comparing the activities of **FRB (1–13)** molecules against various proteins, it has been theoretically proven that these molecules can be used as drugs for human metabolism, and ADME/T analysis was performed to be able to do this test. With this analysis, the movements of molecules in human metabolism are predicted. The entry of the molecule into human metabolism includes many processes, including movements in metabolism and excretion from metabolism, which are called ADME/T, known as Absorption, Distribution, Metabolism, Excretion, and Toxicity, are given in Table 7 [55]. This analysis is divided into two parts. First, the chemical properties of the molecules in the first part and the biological properties of the molecules in the second part are examined.

There are many parameters that examine the chemical properties of molecules, such as mol_MW (mole mass of molecules), dipole (dipole moment), SASA (solvent accessible surface area), volume (molecule volume), donorHB, and accptHB (number of hydrogen bonds that a molecule receives and gives off). parameter is calculated [56]. On the other hand, there are many parameters that examine the biological properties of molecules, which are QPlogHERG (predicted $IC_{50}$ value for blockage of HERG K + channels), QPPCaco and QPPMDCK (blood–brain and blood-bowel barriers), QPlogKp (predicted skin permeability), QPlogKhsa (prediction of binding to human serum albumin), and Human Oral Absorption (predicted qualitative human oral absorption) [57]. Apart from these, there are two parameters, such as Rule Of Five [58] and Rule Of Three [59], that examine the drug feasibility of molecules and are known as Rule Of Five. The quantity of instances in which Lipinski's rule of five and Rule of Three are not adhered to is sometimes referred to as the count of violations of Jorgensen's Rule of Three. The tabulated values in Table 7 demonstrate that the estimated properties of these compounds indicate their potential suitability for human metabolism.

As a result of the calculations, the ADME/T parameters of the molecules were calculated. As a result of these calculations, when the numerical value of the chemical parameters in the ADME/T parameters of the FRB-8 molecule, which is the molecule with the highest activity, is examined, the molecular mass is in the range of 130–725 g/mol, the dipole moment is in the range of 1.0–12.5 D, and the volume is in the range of 500–2000 A3. Both donorHB and accptHB were found to be in the desired range. In addition, when its biological parameters are examined, it has been seen that the QPlogHERG value is desired to be lower than −5 and that there are suitable molecules for blood–brain and blood-intestinal barriers such as QPPCaco and QPPMDCK. At the end of these, the numerical value of two important parameters, such as the rule of five and the rule of three, of the molecules is expected to be zero in order to be a good drug molecule. It is seen that this value is generally zero for all molecules.

## 4. Conclusion

In conclusion, hybrid compounds containing two crucial pharmacophores (the imidazole ring and the hydrazone moiety) were synthesized and biologically evaluated as agents that suppress proliferation and carbonic anhydrase activity in human carbonic anhydrase I and II enzymes. A good number of these compounds demonstrated significant antiproliferative activity and exhibited inhibitory effects on carbonic anhydrase. Particularly, FRB-1, FRB-4, and FRB-8 exhibited the most pronounced cytotoxic effects, which were shown to be comparable to those of a reference commercial drug, Imatinib. In addition, these compounds exhibited noteworthy inhibitory effects when compared to established inhibitors. This is supported by their Ki values, which ranged from 6.49 ± 1.010–739.12 ± 111.35 nM for hCA I (with a Ki value of 271.15 ± 74.620 nM for the standard inhibitor) and 64.53 ± 19.44–314.37 ± 54.78 nM for hCA II (with a Ki value of 113.07 ± 20.980 nM for the standard inhibitor). Furthermore, the active sites of molecules were determined by DFT analysis, and molecular docking results showed that these compounds inhibited hCA I and hCA II enzymes through interactions including H-bonds, p-p stacking, and hydrophobic interactions. Finally, in silico ADME studies have demonstrated that these compounds have a good pharmacokinetic profile. Hence, the outcomes of our study hold potential significance in the identification of forthcoming antiproliferative drugs and carbonic anhydrase inhibitors that exhibit reduced toxicity.

## CRediT authorship contribution statement

**Michael Tapera:** Investigation, Methodology, Conceptualization, Data curation, Visualization, Writing – original draft, Writing – review & editing. **Hüseyin Kekeçmuhammed:** Investigation, Visualization, Data curation. **Emin Sarıpınar:** Supervision. **Murat Doğan:** Investigation, Writing – review & editing. **Burak Tüzün:** Investigation, Visualization, Data curation, Writing – review & editing. **Ümit M. Koçyiğit:** Investigation, Writing – review & editing. **Feyza Nur Çetin:** Investigation, Visualization.

## Declaration of Competing Interest

The authors declare that they have no known competing financial interests or personal relationships that could have appeared to influence the work reported in this paper.

## Data availability

No data was used for the research described in the article.

## Acknowledgements

The authors express a debt of gratitude to Erciyes University's Research Foundation (Grant No: FYL-2021-11122). The authors acknowledge to TUBITAK ULAKBIM for allowing access of their facilities for numerical calculations in this paper.

## Appendix A. Supplementary material

Supplementary data to this article can be found online at https://doi.org/10.1016/j.molliq.2023.123242.

## References

[1] H. Sung, J. Ferlay, R.L. Siegel, M. Laversanne, I. Soerjomataram, A. Jemal, F. Bray, Global Cancer Statistics 2020: GLOBOCAN Estimates of Incidence and Mortality Worldwide for 36 Cancers in 185 Countries, CA. Cancer J. Clin. 71 (2021) 209–249. 10.3322/CAAC.21660.

[2] M. Jadhav, R.S. Kalhapure, S. Rambharose, C. Mocktar, T. Govender, Synthesis, characterization and antibacterial activity of novel heterocyclic quaternary ammonium surfactants, J. Ind. Eng. Chem. 47 (2017) 405–414, https://doi.org/10.1016/j.jiec.2016.12.013.

[3] P. Govindaiah, N. Dumala, I. Mattan, P. Grover, M. Jaya Prakash, Design, synthesis, biological and in silico evaluation of coumarin-hydrazone derivatives as tubulin targeted antiproliferative agents, Bioorg. Chem. 91 (2019), 103143, https://doi.org/10.1016/j.bioorg.2019.103143.

[4] G.F. Zha, H.L. Qin, B.G.M. Youssif, M.W. Amjad, M.A.G. Raja, A.H. Abdelazeem, S. N.A. Bukhari, Discovery of potential anticancer multi-targeted ligustrazine based cyclohexanone and oxime analogs overcoming the cancer multidrug resistance, Eur. J. Med. Chem. 135 (2017) 34–48, https://doi.org/10.1016/j.ejmech.2017.04.025.

[5] S. Ökten, | Ali Aydın, | Ümit, M. Koçyiğit, | Osman Çakmak, | Cenk, A. Andac, | Parham Taslimi, İ. Gülçin, Quinoline-based promising anticancer and antibacterial agents, and some metabolic enzyme inhibitors, Wiley Online Libr. 353 (2020). 10.1002/ardp.202000086.

[6] E. Guzel, U. Kocyigit, P. Taslimi, I. Gulcin, S. Erkan, Phthalocyanine complexes with (4-isopropylbenzyl) oxy substituents: preparation and evaluation of anti-carbonic anhydrase, anticholinesterase enzymes and, (2021).

[7] Ü.M. Koçyiğit, H. Gezegen, P. Taslimi, Synthesis, characterization, and biological studies of chalcone derivatives containing Schiff bases: Synthetic derivatives for the treatment of epilepsy and Alzheimer's disease, Arch. Pharm. (Weinheim). 353 (2020), https://doi.org/10.1002/ardp.202000202.

[8] M. Huseynova, P. Taslimi, A. Medjidov, V. Farzaliyev, M. Aliyeva, G. Gondolova, O. Şahin, B. Yalçın, A. Sujayev, E.B. Orman, A.R. Özkaya, İ. Gulçin, Synthesis, characterization, crystal structure, electrochemical studies and biological evaluation of metal complexes with thiosemicarbazone of glyoxylic acid, Polyhedron 155 (2018) 25–33, https://doi.org/10.1016/j.poly.2018.08.026.

[9] U. Tutar, Ü.M. Koçyiğit, H. Gezegen, Evaluation of antimicrobial, antibiofilm and carbonic anhydrase inhibition profiles of 1,3-bis-chalcone derivatives, J. Biochem. Mol. Toxicol. 33 (2019), https://doi.org/10.1002/jbt.22281.

[10] H. Gezegen, M.B. Gürdere, A. Dinçer, O. Özbek, Ü.M. Koçyiğit, P. Taslimi, B. Tüzün, Y. Budak, M. Ceylan, Synthesis, molecular docking, and biological activities of new cyanopyridine derivatives containing phenylurea, Arch. Pharm. (Weinheim). 354 (2021), https://doi.org/10.1002/ardp.202000334.

[11] I. Ali, M.N. Lone, H.Y. Aboul-Enein, Imidazoles as potential anticancer agents, Medchemcomm. 8 (2017) 1742–1773, https://doi.org/10.1039/c7md00067g.

[12] M. Tapera, H. Kekeçmuhammed, B. Tüzün, E. Sarıpınar, Ü.M. Koçyiğit, E. Yıldırım, M. Doğan, Y. Zorlu, Synthesis, carbonic anhydrase inhibitory activity, anticancer activity and molecular docking studies of new imidazolyl hydrazone derivatives, J. Mol. Struct. 1269 (2022), 133816, https://doi.org/10.1016/J.MOLSTRUC.2022.133816.

[13] Nikitina, P.A., Basanova, E.I., Nikolaenkova, E.B., Os'kina, I.A., Serova, O.A., Bormotov, N.I., Shishkina, L.N., Perevalov, V.P., Tikhonov, A.Ya., 2023. Synthesis of esters and amides of 2-aryl-1-hydroxy-4-methyl-1H-imidazole-5-carboxylic acids and study of their antiviral activity against orthopoxviruses. Bioorganic & Medicinal Chemistry Letters 79, 129080. 10.1016/j.bmcl.2022.129080.

[14] P. Kumar, B.N.-M. reviews in medicinal chemistry, undefined 2013, Hydrazides/hydrazones as antimicrobial and anticancer agents in the new millennium, Ingentaconnect.Com. (n.d.).

[15] Y.L. Fan, X.H. Jin, Z.P. Huang, H.F. Yu, Z.G. Zeng, T. Gao, L.S. Feng, Recent advances of imidazole-containing derivatives as anti-tubercular agents, Eur. J. Med. Chem. 150 (2018) 347–365, https://doi.org/10.1016/j.ejmech.2018.03.016.

[16] R. Gujjarappa, A.K. Kabi, S. Sravani, A. Garg, N. Vodnala, U. Tyagi, D. Kaldhi, R. Velayutham, V. Singh, S. Gupta, C.C. Malakar, Overview on Biological Activities of Imidazole Derivatives, in: Materials Horizons: From Nature to NanoMaterials, Springer Singapore, Singapore, 2022, pp. 135–227.

[17] P. Wattanasin, P. Saetear, P. Wilairat, D. Nacapricha, S. Teerasong, Zone fluidics for measurement of octanol-water partition coefficient of drugs, Anal. Chim. Acta. 860 (2015) 1–7, https://doi.org/10.1016/j.aca.2014.08.025.

[18] L. Zhang, X.-M. Peng, G.L.V. Damu, R.-X. Geng, C.-H. Zhou, Comprehensive Review in Current Developments of Imidazole-Based Medicinal Chemistry, Med. Res. Rev. 34 (2013) 340–437, https://doi.org/10.1002/med.21290.

[19] L. Zhang, X.M. Peng, G.L.V. Damu, R.X. Geng, C.H. Zhou, Comprehensive Review in Current Developments of Imidazole-Based Medicinal Chemistry, Med. Res. Rev. 34 (2014) 340–437, https://doi.org/10.1002/MED.21290.

[20] E.M.H. Ali, M.S. Abdel-Maksoud, U.M. Ammar, K.I. Mersal, K. Ho Yoo, P. Jooryeong, C.H. Oh, Design, synthesis, and biological evaluation of novel imidazole derivatives possessing terminal sulphonamides as potential BRAFV600E inhibitors, Bioorg. Chem. 106 (2021), https://doi.org/10.1016/j.bioorg.2020.104508.

[21] C. Fan, T. Zhong, H. Yang, Y. Yang, D. Wang, X. Yang, Y. Xu, Y. Fan, Design, synthesis, biological evaluation of 6-(2-amino-1H-benzo[d]imidazole-6-yl)quinazolin-4(3H)-one derivatives as novel anticancer agents with Aurora kinase inhibition, Eur. J. Med. Chem. 190 (2020), 112108, https://doi.org/10.1016/j.ejmech.2020.112108.

[22] L. Li, D. Quan, J. Chen, J. Ding, J. Zhao, L. Lv, J. Chen, Design, synthesis, and biological evaluation of 1-substituted -2-aryl imidazoles targeting tubulin polymerization as potential anticancer agents, Eur. J. Med. Chem. 184 (2019), https://doi.org/10.1016/j.ejmech.2019.111732.

[23] M.A. Assiri, A. Ali, M. Ibrahim, M.U. Khan, K. Ahmed, M.S. Hamid Akash, M. A. Abbas, A. Javed, M. Suleman, M. Khalid, I. Hussain, Potential anticancer and antioxidant lauric acid-based hydrazone synthesis and computational study toward the electronic properties, RSC Adv. 13 (2023) 21793–21807, https://doi.org/10.1039/d3ra02433d.

[24] H. Kekeçmuhammed, M. Tapera, B. Tüzün, S. Akkoç, Y. Zorlu, E. Sarıpınar, Synthesis, Molecular Docking and Antiproliferative Activity Studies of a Thiazole-Based Compound Linked to Hydrazone Moiety, ChemistrySelect. 7 (2022) e202201502. 10.1002/SLCT.202201502.

[25] H. Kekeçmuhammed, M. Tapera, E. Aydoğdu, E. Sarıpınar, E. Aydin Karatas, E. Mehtap Uc, M. Akyuz, B. Tüzün, İ. Gulcin, R. Emin Bora, İ. Özer İlhan, Synthesis, Biological Activity Evaluation and Molecular Docking of Imidazole Derivatives Possessing Hydrazone Moiety, Chem. Biodivers. 20 (2023) e202200886. 10.1002/cbdv.202200886.

[26] M. Tapera, H. Kekeçmuhammed, C.U. Tunc, A.U. Kutlu, İ. Çelik, Y. Zorlu, O. Aydin, E. Sarıpınar, Design, synthesis, molecular docking and biological evaluation of 1,2,4-triazole derivatives possessing a hydrazone moiety as anti-breast cancer agents, New J. Chem. 47 (2023) 11602–11614, https://doi.org/10.1039/d3nj01320k.

[27] Y. Demir, F.S. Tokalı, E. Kalay, C. Türkeş, P. Tokalı, O.N. Aslan, K. Şendil, Ş. Beydemir, Synthesis and characterization of novel acyl hydrazones derived from vanillin as potential aldose reductase inhibitors, Mol. Divers. 27 (2022) 1713–1733, https://doi.org/10.1007/s11030-022-10526-1.

[28] M. Tapera, H. Kekeçmuhammed, K. Sahin, V.S. Krishna, C. Lherbet, H. Homberset, M. Chebaiki, T. Tønjum, L. Mourey, Y. Zorlu, S. Durdagi, E. Sarıpınar, Synthesis, characterization, anti-tuberculosis activity and molecular modeling studies of thiourea derivatives bearing aminoguanidine moiety, J. Mol. Struct. 1270 (2022), https://doi.org/10.1016/j.molstruc.2022.133899.

[29] R. Kaplánek, M. Jakubek, J. Rak, Z. Kejík, M. Havlík, B. Dolenský, I. Frydrych, M. Hajdúch, M. Kolář, K. Bogdanová, J. Králová, P. Džubák, V. Král, Caffeine-hydrazones as anticancer agents with pronounced selectivity toward T-lymphoblastic leukaemia cells, Bioorg. Chem. 60 (2015) 19–29, https://doi.org/10.1016/j.bioorg.2015.03.003.

[30] F. Chimenti, B. Bizzarri, E. Maccioni, D. Secci, A. Bolasco, P. Chimenti, R. Fioravanti, A. Granese, S. Carradori, F. Tosi, P. Ballario, S. Vernarecci, P. Filetici, A novel histone acetyltransferase inhibitor modulating Gcn5 network: cyclopentylidene-[4-(4'-chlorophenyl)thiazol-2-yl)hydrazone, J. Med. Chem. 52 (2009) 530–536, https://doi.org/10.1021/jm800885d.

[31] Y. Wang, G. Zhang, G. Hu, Y. Bu, H. Lei, D. Zuo, M. Han, X. Zhai, P. Gong, Design, synthesis and biological evaluation of novel 4-arylaminopyrimidine derivatives

possessing a hydrazone moiety as dual inhibitors of L1196M ALK and ROS1, Eur. J. Med. Chem. 123 (2016) 80–89, https://doi.org/10.1016/j.ejmech.2016.06.056.
[32] A. Tas, B. Tüzün, A.N. Khalilov, P. Taslimi, T. Ağbektas, N.K. Cakmak, In vitro cytotoxic effects, in silico studies, some metabolic enzymes inhibition, and vibrational spectral analysis of novel β-amino alcohol compounds, J. Mol. Struct. 1273 (2023), https://doi.org/10.1016/j.molstruc.2022.134282.
[33] M.J. Frisch, et al., Gaussian16 Revision B.01, Gaussian Inc., Wallingford CT, 2016.
[34] Schrödinger Release 2019-4.
[35] M.R. Aouad, M. Messali, N. Rezki, N. Al-Zaqri, I. Warad, Single proton intramigration in novel 4-phenyl-3-((4-phenyl-1H-1,2,3-triazol-1-yl)methyl)-1H-1,2,4-triazole-5(4H)-thione: XRD-crystal interactions, physicochemical, thermal, Hirshfeld surface, DFT realization of thiol/thione tautomerism, J. Mol. Liq. 264 (2018) 621–630, https://doi.org/10.1016/j.molliq.2018.05.085.
[36] D. Vautherin, D.M. Brink, Hartree-fock calculations with skyrme's interaction. I. Spherical nuclei, Phys. Rev. C. 5 (1972) 626–647, https://doi.org/10.1103/PhysRevC.5.626.
[37] H. Doğan, Ş.D. Doğan, M.G. Gündüz, V.S. Krishna, C. Lherbet, D. Sriram, O. Şahin, E. Sarıpınar, Discovery of hydrazone containing thiadiazoles as Mycobacterium tuberculosis growth and enoyl acyl carrier protein reductase (InhA) inhibitors, Eur. J. Med. Chem. 188 (2020), 112035, https://doi.org/10.1016/j.ejmech.2020.112035.
[38] T. Taskin, M. Dogan, T. Arabaci, Bioassay-guided isolation and antiproliferative efficacy of extract loaded in chitosan nanoparticles and LC-QTOF-MS/MS analysis of Achillea magnifica, South African J. Bot. 133 (2020) 236–244, https://doi.org/10.1016/j.sajb.2020.08.002.
[39] U. Tutar, | Ümit, M. Koçyiğit, | Hayreddin Gezegen, Ü.M. Koçyiğit, Evaluation of antimicrobial, antibiofilm and carbonic anhydrase inhibition profiles of 1, 3-bis-chalcone derivatives, Wiley Online Libr. 33 (2018). 10.1002/jbt.22281.
[40] Ü.M. Koçyiğit, Sıçanların Kalp Dokusunda Oksitosin'in Karbonik Anhidraz ve Asetilkolinesteraz Enzimleri Üzerine İnhibisyon Etkisinin Araştırılması, J. Inst Sci. Technol. 8 (2018) 199–207, https://doi.org/10.21597/jist.407875.
[41] N. Doğan, S.Ç. Yavuz, K. Sahin, M.D. Orhan, H.K. Muhammed, S. Calis, F.Ö. Küp, T. Avsar, S. Akkoc, M. Tapera, O. Sahin, T. Kilic, S. Durdagi, E. Saripinar, Synthesis, Characterization, Biological Activity and Molecular Modeling Studies of Novel Aminoguanidine Derivatives, ChemistrySelect 7 (2022), https://doi.org/10.1002/slct.202202819.
[42] I.A.S. Al-Janabi, S.Ç. Yavuz, S. Köprü, M. Tapera, H. Kekeçmuhammed, S. Akkoç, B. Tüzün, Ş. Patat, E. Sarıpınar, Antiproliferative activity and molecular docking studies of new 4-oxothiazolidin-5-ylidene acetate derivatives containing guanylhydrazone moiety, J. Mol. Struct. 1258 (2022), 132627, https://doi.org/10.1016/j.molstruc.2022.132627.
[43] S. Çağlar Yavuz, S. Akkoç, B. Türkmenoğlu, E. Sarıpınar, Synthesis of novel heterocyclic compounds containing pyrimidine nucleus using the Biginelli reaction: Antiproliferative activity and docking studies, J. Heterocycl. Chem. 57 (2020) 2615–2627, https://doi.org/10.1002/jhet.3978.
[44] V. Štrukil, D. Margetic, M.D. Igrc, M. Eckert-Maksic, T. Friščic, Desymmetrisation of aromatic diamines and synthesis of non-symmetrical thiourea derivatives by click-mechanochemistry, Chem. Commun. 48 (2012) 9705–9707, https://doi.org/10.1039/c2cc34013e.
[45] S. Varun, R. Kakkar, Isatin and its derivatives: a survey of recent syntheses, reactions, and applications, Medchemcomm. 10 (2019) 351–368, https://doi.org/10.1039/c8md00585k.
[46] G. Sarkı, B. Tüzün, D. Ünlüer, H. Kantekin, Synthesis, characterization, chemical and biological activities of 4-(4-methoxyphenethyl)-5- benzyl-2-hydroxy-2H-1,2,4-triazole-3(4H)-one phthalocyanine derivatives, Inorganica Chim. Acta. 545 (2023), https://doi.org/10.1016/j.ica.2022.121113.
[47] M. Chalkha, A. Ameziane el Hassani, A. Nakkabi, B. Tüzün, M. Bakhouch, A. T. Benjelloun, M. Sfaira, M. Saadi, L. El Ammari, M. El Yazidi, Crystal structure, Hirshfeld surface and DFT computations, along with molecular docking investigations of a new pyrazole as a tyrosine kinase inhibitor, J. Mol. Struct. 1273 (2023), https://doi.org/10.1016/j.molstruc.2022.134255.
[48] M.S. Çelik, Ş.A. Çetinus, A.F. Yenidünya, S. Çetinkaya, B. Tüzün, Biosorption of Rhodamine B dye from aqueous solution by Rhus coriaria L. plant: Equilibrium, kinetic, thermodynamic and DFT calculations, J. Mol. Struct. 1272 (2023), https://doi.org/10.1016/j.molstruc.2022.134158.
[49] I. Shahzadi, A.F. Zahoor, A. Rasul, A. Mansha, S. Ahmad, Z. Raza, Synthesis, hemolytic studies, and in silico modeling of novel acefylline-1,2,4-triazole hybrids as potential anti-cancer agents against MCF-7 and A549, ACS Omega 6 (2021) 11943–11953, https://doi.org/10.1021/acsomega.1c00424.
[50] P. Taslimi, F. Akhundova, M. Kurbanova, F. Türkan, B. Tuzun, A. Sujayev, N. Sadeghian, A. Maharramov, V. Farzaliyev, İ. Gülçin, Biological Activity and Molecular Docking Study of Some Bicyclic Structures: Antidiabetic and Anticholinergic Potentials, Polycycl. Aromat. Compd. 42 (2022) 6003–6016, https://doi.org/10.1080/10406638.2021.1981405.
[51] A. Poustforoosh, H. Hashemipour, B. Tüzün, M. Azadpour, S. Faramarz, A. Pardakhty, M. Mehrabani, M.H. Nematollahi, The Impact of D614G Mutation of SARS-COV-2 on the Efficacy of Anti-viral Drugs: A Comparative Molecular Docking and Molecular Dynamics Study, Curr. Microbiol. 79 (2022), https://doi.org/10.1007/s00284-022-02921-6.
[52] A. Mermer, M. Volkan Bulbul, S. Mervenur Kalender, I. Keskin, B. Tuzun, O. Emre Eyupoglu, Benzotriazole-oxadiazole hybrid Compounds: Synthesis, anticancer Activity, molecular docking and ADME profiling studies, J. Mol. Liq. 359 (2022), 119264, https://doi.org/10.1016/j.molliq.2022.119264.
[53] Y. Lakhrissi, M. Rbaa, B. Tuzun, A. Hichar, E.H. Anouar, K. Ounine, F. Almalki, T. Ben Hadda, A. Zarrouk, B. Lakhrissi, Synthesis, structural confirmation, antibacterial properties and bio-informatics computational analyses of new pyrrole based on 8-hydroxyquinoline, J. Mol. Struct. 1259 (2022), https://doi.org/10.1016/j.molstruc.2022.132683.
[54] B.K. Kumar, K.V.G.C. Faheem, R. Sekhar, V.K. Ojha, A. Prajapati, S. Pai, Murugesan, Pharmacophore based virtual screening, molecular docking, molecular dynamics and MM-GBSA approach for identification of prospective SARS-CoV-2 inhibitor from natural product databases, J. Biomol. Struct. Dyn. 40 (2022) 1363–1386, https://doi.org/10.1080/07391102.2020.1824814.
[55] B. Tüzün, K. Sayïn, H. Ataseven, Could Momordica Charantia Be Effective In The Treatment of COVID19?, Cumhur, Sci. J. 43 (2022) 211–220, https://doi.org/10.17776/csj.1009906.
[56] M. Rbaa, S. Haida, B. Tuzun, A. Hichar, A. El Hassane, A. Kribii, Y. Lakhrissi, T. Ben Hadda, A. Zarrouk, B. Lakhrissi, E. Berdimurodov, Synthesis, characterization and bioactivity of novel 8-hydroxyquinoline derivatives: Experimental, molecular docking, DFT and POM analyses, J. Mol. Struct. 1258 (2022), https://doi.org/10.1016/j.molstruc.2022.132688.
[57] M.A. Bhat, B. Tüzün, N.A. Alsaif, A. Ali Khan, A.M. Naglah, Synthesis, characterization, molecular modeling against EGFR target and ADME/T analysis of novel purine derivatives of sulfonamides, J. Mol. Struct. 1257 (2022), 132600, https://doi.org/10.1016/J.MOLSTRUC.2022.132600.
[58] M.-Q. Zhang, B. Wilkinson, Drug discovery beyond the 'rule-of-five', Curr. Opin. Biotechnol. 18 (2007) 478–488, https://doi.org/10.1016/j.copbio.2007.10.005.
[59] Colombo, S., 2020. Applications of artificial intelligence in drug delivery and pharmaceutical development, in: Artificial Intelligence in Healthcare. Elsevier, pp. 85–116.